Assessment of the validity of some common assumptions in hygrothermal modelling of earth based materials

Soudani , L. , Fabbri , A. , Morel, J. C. , Woloszyn , M , Chabriac, P. A. , Wong, H. and Grillet, A. C.

Original citation & hyperlink:
Soudani , L. , Fabbri , A. , Morel, J. C. , Woloszyn , M , Chabriac, P. A. , Wong, H. and Grillet, A. C. (2016) Assessment of the validity of some common assumptions in hygrothermal modelling of earth based materials. *Energy and Buildings*, volume 116 : 498–511
http://dx.doi.org/10.1016/j.enbuild.2016.01.025

DOI 10.1016/j.enbuild.2016.01.025
ISSN 0378-7788

Publisher: Elsevier

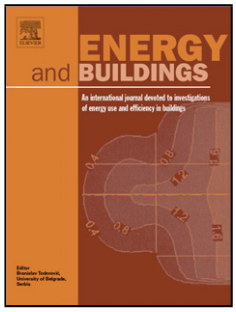

Title: Assessment of the validity of some common assumptions in hygrothermal modelling of earth based materials

Author: Lucile Soudani Antonin Fabbri Jean-Claude Morel Monika Woloszyn Pierre-Antoine Chabriac Henry Wong Anne-Cécile Grillet

PII: S0378-7788(16)30025-1
DOI: http://dx.doi.org/doi:10.1016/j.enbuild.2016.01.025
Reference: ENB 6399

To appear in: *ENB*

Received date: 19-3-2014
Revised date: 21-12-2015
Accepted date: 19-1-2016

Please cite this article as: L. Soudani, A. Fabbri, J.-C. Morel, M. Woloszyn, P.-A. Chabriac, H. Wong, A.-C. Grillet, Assessment of the validity of some common assumptions in hygrothermal modelling of earth based materials, *Energy and Buildings* (2016), http://dx.doi.org/10.1016/j.enbuild.2016.01.025

Assessment of the validity of some common assumptions in hygrothermal modelling of earth based materials

Lucile Soudani[a,b], Antonin Fabbri[a*], Jean-Claude Morel[c], Monika Woloszyn[b], Pierre-Antoine Chabriac[d], Henry Wong[a], Anne-Cécile Grillet[b]

[a]LGCB-LTDS, UMR 5513 CNRS, ENTPE, Université de Lyon, 69100 Vaulx-en-Velin, France
[b]LOCIE, CNRS-UMR 5271, Université Savoie Mont Blanc, Campus Scientifique, Savoie Technolac, 73376 Le Bourget-du-Lac Cedex, France
[c]School of Energy, Construction and Environment, Faculty of Engineering, Environment & Computing, Coventry University, UK
[b]Ecole Nationale Supérieure d'Architecture de Saint-Étienne, 42003 Saint-Étienne Cedex 1, France

*. Tel.: 33 472 047 286; fax: 33 472 047 156, Email: antonin.fabbri@entpe.fr

Abstract

The goal of this paper is to identify the effects of in-pore transport of liquid water and water vapor as well as phase changes on the hygrothermal behavior of earthen buildings. Indeed, one of the main assets used to promote these constructions is their role in moisture buffering hence temperature and relative-humidity quality controlling. However, there is no clear consensus yet concerning the impact of these phenomena on the global energy performance of the buildings. A coupled model is therefore proposed in this paper, based on heat and mass balances inside the earthen walls, in order to clarify this question. This model considers separately the kinematics of each phase (e.g. liquid water, vapor, dry air and solid matrix), in interaction with each other. It also takes into account the impact of pore water confinement on the liquid-to-vapor phase change, in particular on the resulting latent heat released or absorbed. The model is successfully compared to experimental results on instrumented full-scale rammed earth wall subjected to temperature cycles. It eventually allows identifying the singular hygrothermal behaviour of earth material by testing the range of applicability of the simplifying assumptions which are commonly made in function of the permeability of the tested material.

Keywords

Heat and moisture transport, Hygrothermal modeling, Numerical simulation, Rammed earth, Adobe, Cob

Nomenclature

LATIN NOTATION

C_{LG}	m^{-1}	Curvature of the interface
$C_{p,A}$	$J.kg^{-1}.K^{-1}$	Air specific heat capacity at constant pressure
$C_{p,L}$	$J.kg^{-1}.K^{-1}$	Liquid specific heat capacity at constant pressure
$C_{p,S}$	$J.kg^{-1}.K^{-1}$	Specific heat capacity of the dry material at constant pressure
$C_{p,V}$	$J.kg^{-1}.K^{-1}$	Vapor specific heat capacity at constant pressure
D_e^V	$m^2.s^{-1}$	Effective diffusion coefficient
L	$J.kg^{-1}$	Integral enthalpy of evaporation per unit of mass
m_I	$kg.m^{-3}$	Mass of component I per unit of representative elementary volume of porous material
$\overset{\circ}{m}_{\rightarrow V}$	$kg.s^{-1}$	Rate of vapor mass production due to phase changes
M_{H_2O}	$kg.mol^{-1}$	Molar mass of water
p_G	Pa	Gas pressure
p_L	Pa	Liquid pressure
p_V^{sat}	Pa	Equilibrium vapor pressure
R	$J.K^{-1}.mol^{-1}$	Gas constant
S_r	-	Saturation ratio
T	K	temperature
T_{ref}	K	Reference temperature
V_G	$m.s^{-1}$	Relative gaseous phase velocity in the porous media
V_V	$m.s^{-1}$	Relative water vapor velocity in the porous media
w	$kg.kg^{-1}$	Mass water content

GREEK NOTATION

α	W.m^{-2}.K^{-1}	heat transfer coefficient
α_L		thermal volume dilatation coefficient of the liquid
β	kg.m^{-2}.s^{-1}.Pa^{-1}	moisture transfer coefficient
γ_{LG}	N.m^{-1}	Interfacial tension between liquid water and air
η_L	Pa.s	dynamic viscosity of water
κ	m^2	intrinsic permeability of the porous medium
κ_r^L	-	relative liquid permeability
λ	W.m^{-1}.K^{-1}	thermal conductivity
ρ_d	kg.m^{-3}	density of the dry material
ρ_L	kg.m^{-3}	water density
ρ_G	kg.m^{-3}	density of the gaseous mixture
ρ_V	kg.m^{-3}	Mass concentration of vapor in wet air
ρ_A	kg.m^{-3}	Mass concentration of dry air in wet air
φ	-	relative humidity
ϕ	-	porosity
ϕ_L	-	porosity filled by the liquid phase

#body

1. INTRODUCTION

The stabilization of the atmospheric greenhouse gas concentration requires our emissions to drop well below current levels, and thus to reduce drastically our energy consumption. In this context, the building sector plays a key role, as it accounts for about 40% of their generation [1].

Consequently, increasing research has been performed on the thermal insulation of buildings in order to optimize and reduce energy consumption. This approach is effectively a possible way to reduce energy losses from buildings made with industrially manufactured materials. Nowadays, several materials and techniques are available and their performances are well established.

However, most of these building materials, either for insulation (such as glass fiber) or for wall manufacturing (such as concrete), are major energy consumers during both their production and implementation (embodied energy), and their recycling is not always operational [2]. Consequently, the development of earth-based buildings appears to be a sustainable alternative to conventional constructions [3]. Indeed, the major interest of earth lies in the fact that it is a local material that can be produced and used immediately on the construction site or nearby and does not require industrial processing. It is not a renewable but a reusable material; it requires no treatment to be reused and therefore has a very low impact in terms of energy consumption [4].

In addition, one of the main assets of earthen materials is its role in moisture buffering and temperature controlling, which can be related to phase change processes occurring within the pores [5][6]. This is due to the microstructure of the earth which enables hydric exchanges with the environment through condensation/evaporation and sorption/desorption phenomena of water molecules on the pore surfaces [7]. These variations in water content can also significantly modify the apparent thermal conductivity and the thermal capacity of the material [8]. Several researches focused on the experimental quantification of these transfers and their modeling (eg. [9] or [10] and [11]).

However, this task is not simple as the load-bearing walls act as barriers between drastically different environments (e.g. indoor, outdoor, foundation and roof). They are subjected to strong thermal and hydric gradients leading to migration of liquid water and water vapor at different temperatures. A proper modeling of the behavior of the interstitial fluid is thus essential to assess the energy performance and the control capacity of temperature and relative humidity of earthen constructions [11],[12],[13]. A synthetic representation of the coupling between thermal and hydrodynamic processes is reported in **Error! Reference source not found.**.

If all these physical processes and couplings are theoretically well known in the scientific community, their integration into a complete and consistent model and the implementation of the latter in a code of hygrothermal calculations remains a major scientific and technical challenge.

To reach this goal, some authors [14],[15] do start from a microscopic scale and reach the macroscopic scale by averaging on a representative volume. This allows a better appraisal of the assumptions required. Others [16], [17], [18] have adopted a phenomenological approach enabling them to deal with physical problems right from the macroscopic scale. This latter even gave rise to commercially developed software [19],[20] which can provide reliable results on a wide range of materials and climatic loads [14],[15].

However, we can wonder whether these models, which are based on simplified transport and storage functions, are able to reproduce with accuracy the hygrothermal behavior of unconventional material like earth, when they are submitted to important hygrometry and temperature variations.

The aim of this paper is firstly to quantify the influence of particular assumptions made while deriving the governing equations, and secondly to examine their degree of relevance when applied to the study of the hygrothermal behavior of earthen materials in relation to their hydric characteristics. The refinements introduced in the development of this coupled model enable precise studies of the processes occurring in this type of materials and the range of applicability of some commonly made assumptions in hygrothermal models.

2. HYGROTHERMAL MODEL SET-UP

In this paper, the rammed earth is modelled as the superposition of a solid skeleton (*S)* and a porous network partially saturated by liquid water (*L)*, assumed to be pure. The remaining porous network space is filled by a continuous gaseous phase (*G)*, which is assumed to be an ideal mixture of perfect gases composed of dried air (*A)* and water vapor (*V)*. The porosity (ϕ) is defined as the actual volume of porous network per unit of initial volume of

rammed earth, while the water saturation ratio (S_r), is defined as the actual volume of liquid water per unit of actual porous volume. This latter is linked to the liquid water content ($w_L = m_L / m_S$, where m_L and m_S are respectively the liquid and skeleton masses per unit of rammed earth volume), through:

$$S_r = w_L \frac{\rho_d}{\phi \rho_L} \quad (1)$$

where ρ_d is density of the dried earthen material and ρ_L is the water density.

Let us note that the water content can also be defined as the total mass of water (liquid and vapor) per unit of skeleton mass ($w = \left(m_L + m_V\right) / m_S$). However, since $m_L \gg m_V$, the difference between the two definitions remains of third order. In the following, the use of w_L is preferred because it allows a direct link between the saturation ratio and the water content.

The proportion of dry air (A) and water vapor (V) within the gaseous phase (G) is quantified by their mass concentration ρ_I , where $I = A, V$, defined as:

$$\rho_I = \frac{m_I}{\left(1 - S_r\right)\phi}; \rho_G = \sum_{I=A,V} \rho_I \quad (2)$$

where m_I is the mass of $I = A,V$ per unit of representative elementary volume of rammed earth, and ρ_G is the density of the gaseous mixture. Finally, an exchange of matter can occur between phases *L* and *V*, due to condensation of the water vapor and evaporation of liquid water.

A schematic representation of the porous medium is reported in **Error! Reference source not found.**.

2.1. Liquid water - vapor equilibrium

A decrease (resp. increase) of water content in the porous network leads to an increase (resp. decrease) of the liquid/air interface curvature. The latter is commonly assumed to be close to the inverse of the entry radius of the pores where the evaporation (resp. condensation) process occurs. It leads to a variation of the capillary pressure (or suction) defined as:

$$p_G - p_L = \gamma_{LG} C_{LG} = \mathrm{f}\left(w_L\right) \quad (3)$$

where γ_{LG} is the interfacial tension between the liquid water and air, C_{LG} is the curvature of the interface, p_G and p_L are respectively the air and the liquid water pressures, and $\mathrm{f}\left(w_L\right)$ is a decreasing function of the liquid water content that depends on the porous network characteristic of the material. According to this definition, a decrease in liquid water content leads to a decrease in liquid pressure at constant air pressure. In consequence, the local equilibrium between in-pore confined liquid water (L) and its vapor (V) is modified, and the partial pressure of vapor within the wet air in equilibrium with the liquid water is no more equal to the saturated vapor pressure. Assuming that the total pressure of the gaseous phase p_G remains constant, this modification is expressed through the celebrated Kelvin's Law, which comes from the local equality of the specific free enthalpy of these two phases at the vicinity of their interface [21]:

$$p_G - p_L = -\frac{\rho_L RT}{M_{H_2O}} \ln \varphi \quad (4)$$

Where p_G and p_L are resp. the gas and liquid pressures, ρ_L the density of liquid water, M_{H_2O} its molar mass, R the perfact gaz constant, T the actual temperature and φ the relative humidity, defined as:

$$\varphi = \frac{p_V}{p_V^{sat}} \quad (5)$$

with p_V the partial pressure of vapor within the gaseous phase, and p_V^{sat} the saturated vapor pressure at the current temperature. Under the small perturbation assumption, this latter can be estimated by [21]:

$$p_V^{sat} = p_V^{sat}\left(T_{ref}\right) \exp\left[\frac{M_{H_2O}}{RT}\left[\frac{L_{ref}}{T_{ref}}\left(T - T_{ref}\right) + \left(C_{p,V} - C_{p,L}\right)\right] T \ln\left[\frac{T}{T_{ref}}\right] - \left(T - T_{ref}\right)\right] \quad (6)$$

where L_{ref} is the latent heat of evaporation/condensation at T_{ref} and $p_G = p_L = 1$ bar (for water at T_{ref} = 373 K, $L_{ref} = 2.26 \times 10^6$ J/kg, and $p_V^{sat}\left(T_{ref}\right) = 1\text{bar}$ [21]). Finally, $C_{p,V}$ and $C_{p,L}$ are resp. the vapor and liquid specific heat at constant pressure.

Differentiation of the Kelvin Law and the vapor pressure then leads to the two following equations:

$$\mathrm{d}p_L = \frac{\rho_L R T}{M_{\mathrm{H_2O}}}\mathrm{d}(\ln\varphi) + \frac{\rho_L R \ln\varphi}{M_{H_2O}}\mathrm{d}T$$

$$\mathrm{d}p_V = p_V^{sat}(T)\mathrm{d}\varphi + \varphi\frac{\mathrm{d}p_V^{sat}}{\mathrm{d}T}\mathrm{d}T \quad (7)$$

The combination between (3) and (4) underlines that the water content of a material is linked, at constant temperature and at equilibrium, to the relative humidity of the surrounding air. This link is different for each tested material and can be experimentally determined through sorption and desorption tests.

2.2. Water continuity equation

2.2.1. Water vapor mass balance

Assuming no air flow within the porous network, the mass conservation of water vapor reads:

$$\frac{\partial m_V}{\partial t} = -\nabla\cdot\left(\rho_V \phi_G \left(\underline{V_V} - \underline{V_G}\right)\right) + \overset{\circ}{m}_{\to V} \quad (8)$$

where $\overset{\circ}{m}_{\to V}$ is the rate of vapor mass production due to evaporation/condensation processes. The term $\rho_V \phi_G \left(\underline{V_V} - \underline{V_G}\right)$, where $\underline{V_V}$ is the velocity of the water vapor, $\underline{V_G}$ the velocity of the gaseous phase, stands for the diffusive transport of water vapor within the gaseous phase. This latter can be evaluated through the Fick Law that is expressed in terms of vapor partial pressure [22]:

$$\phi_G\left(\underline{V_V}-\underline{V_G}\right)=-\frac{p_G}{p_V}D_e^V\underline{\nabla}\ \frac{p_V}{p_G} \quad (9)$$

where D_e^V is the effective diffusion coefficient.

Recalling that the water vapor follows the perfect gas relation and that gas pressure variations are neglected, (9) allows to express the vapor mass conservation as:

$$\frac{\partial m_V}{\partial t}=\underline{\nabla}\cdot\ \frac{M_{H_2O}}{RT}D_e^V\underline{\nabla}\left(p_V\right)+\dot{m}_{\to V} \quad (10)$$

2.2.2. Liquid water mass balance

The conservation of the liquid water mass (m_L) is written as:

$$\frac{\partial m_L}{\partial t}=\rho_L\underline{\nabla}\cdot\left(\phi_L\underline{V_L}\right)-\dot{m}_{\to V} \quad (11)$$

where $\phi_L\underline{V_L}$ is the filtration velocity of liquid within the porous material, which is assumed to follow the generalized Darcy law:

$$\phi_L \underline{V}_L = -\frac{\kappa \kappa_r^L}{\eta_L} \underline{\nabla} p_L \quad (12)$$

where $\phi_L = S_r \phi$ is the porosity filled by the liquid phase, κ is the intrinsic permeability of the porous medium, κ_r^L the relative liquid permeability, η_L the dynamic viscosity of water.

2.2.3. Equation of water mass transfer

2.2.3.1. Choice of the driving potential for water transport

Water in the material is present both as liquid and vapor, and these two phases can migrate through the porous medium. However, due to the equilibrium assumption expressed by eq. (4), these two mass transfers are linked to one another, and the global water mass balance can be assessed by a sole equation. The question that arises is the choice of the variable associated to the hydric state of the material. This latter can be the liquid pressure, the vapor pressure, the liquid water content or the relative humidity. Actually, the scope of this model is to reproduce the behavior of a porous wall in the hygroscopic domain where the water content of the material remains quite low. In consequence, the relative permeability of the liquid water is very small and the mass transport of water is mainly due to the gradient of vapor pressure. Then, the use of the vapor pressure or of the relative humidity is found to be the most natural option. The choice of the relative humidity is finally made as it is the physical value commonly measured by hygrothermal sensors.

2.2.3.2. Total water mass balance

Using φ and T as variables, the combination of (1) and (6-8), while neglecting the variation of water content with temperature at constant humidity, and accounting for $\rho_v / \rho_L \ll 1$, the balance of the overall water mass ($m_{H_2O} = m_L + m_V = \phi S_r \rho_L + \phi(1 - S_r)\rho_V$) reads:

$$\frac{1}{\rho_L}\left(\rho_d \frac{\partial w_L}{\partial \varphi} + \phi_G \frac{M_{H_2O} p_v^{sat}(T)}{RT}\right)\frac{\partial \varphi}{\partial t} + \frac{\phi_G \rho_V^{\alpha}}{\rho_L}\frac{\partial T}{\partial t} = \underline{\nabla}\cdot\left(\delta_T \underline{\nabla} T + \delta_{\varphi} \underline{\nabla}\varphi\right) \quad (13)$$

where

$$\rho_V^{\alpha} = \varphi \frac{p_V^{sat}(T) M_{H_2O}}{RT}\left(\frac{1}{p_V^{sat}(T)}\frac{dp_V^{sat}(T)}{dT} - \frac{1}{T}\right) \quad (14)$$

$$\delta_T = \delta_{T1} + \delta_{T2} = \frac{\kappa \kappa_r^L}{\eta_L}\frac{\rho_L R}{M_{H_2O}}\ln\varphi + D_e^V \frac{\varphi M_{H_2O}}{\rho_L RT}\frac{dp_V^{sat}(T)}{dT} \quad (15)$$

$$\delta_{\varphi} = \frac{\kappa \kappa_r^L}{\eta_L}\frac{\rho_L RT}{M_{H_2O}\varphi} + D_e^V \frac{M_{H_2O}}{\rho_L RT} p_V^{sat}(T) \quad (16)$$

The main differences between (13) and the water mass balance equation classically used in hygrothermal models [17] come from the expression of the source term due to temperature variations ($\frac{\phi_G \rho_V^{\alpha}}{\rho_L}\frac{\partial T}{\partial t} - \underline{\nabla}\cdot\delta_T \underline{\nabla} T$).

Indeed, it is commonly assumed that the variation of liquid pressure with temperature at constant hygrometry is negligible, so that the liquid flow becomes exclusively driven by moisture gradient. Under this assumption, the term $\frac{\kappa\kappa_r^L}{\eta_L}\frac{\rho_L R}{M_{H_2O}}\ln\varphi$ vanishes and ^{T} is reduced to $D_e^V\frac{\varphi M_{H_2O}}{\rho_L RT}\frac{dp_V^{sat}(T)}{dT}$.

According to many authors [17], under practical conditions the influence of this assumption is disregarded, but caution should be taken when strong temperature variations occur in the material.

The influence of this “liquid flow only driven by moisture content gradient” assumption will be discussed more in detail in the following.

2.3. Equation of heat transfer

2.3.1 Thermal balance

The entropy balance (see Appendix 2) of the wall leads to the thermal equation in its classical form for porous media with in-pore water phase change [23]. We assume here the enthalpy variation due to sorption/desorption mechanisms to be negligible in comparison with enthalpy variation due to evaporation/condensation:

$$\rho C_p\frac{\partial T}{\partial t}=\underline{\nabla}\cdot\left(\lambda\underline{\nabla}T\right)-\overset{\circ}{m}_{\to V}L(T,\varphi) \quad (17)$$

where λ is the thermal conductivity and ρC_p the average heat capacity at constant pressure given by:

$$\rho C_p = (1-\phi)\rho_S C_{p,S} + \phi S_r \rho_L C_{p,L} + \phi(1-S_r)\left(\rho_A C_{p,A} + \rho_V C_{p,V}\right) \quad (18)$$

where ρ_S, ρ_L are respectively the intrinsic densities of solid matrix and liquid water, while ρ_A and ρ_V are the mass concentrations of air and water vapor within the gas phase (i.e. mass of the constituent per unit volume of the gas phase). $C_{p,S}, C_{p,L}, C_{p,A}, C_{p,V}$ are specific heats at constant pressure of the solid, liquid water, air and water vapor. α_L is the thermal volume dilatation coefficient of the liquid.

Finally, L is the integral enthalpy of evaporation per unit of mass. It varies with respect to temperature, liquid pressure and vapor pressure [24]. Using (4) (i.e. the Kelvin's law), it can be expressed as follows as a function of temperature and equilibrium relative humidity [see Appendix 1]

$$L(T,\varphi) = L_{ref} + \left(C_{p,V} - C_{p,L}\right)\left(T - T_{ref}\right) - \frac{RT}{M_{H_2O}} \ln \varphi \quad (19)$$

Let us underline here that the relative humidity reported in (19), is the relative humidity at equilibrium between the in-pore water and its vapor, which satisfies the Kelvin's law. The last term of (19), leads to an increase of L when the equilibrium relative humidity decrease. It allows considering the effect on the enthalpy of evaporation of the linear reduction of p_V and of the strong reduction of p_L (according to eq. (4)) when the equilibrium relative humidity is reduced (and reciprocally for condensation when the relative humidity increases).

This term is almost always neglected. However, as it is illustrated in **Error! Reference source not found.**, the variations of L with T and φ appears to be on the same order of magnitude. There is thus no apparent reason to justify such simplification and we will therefore keep the entire expression.

2.3.2 Evaluation of the evaporation/condensation rate

To solve the system of partial differential equations (13), (17), we need an additional relation on the evaporation/condensation rate. Assuming that the kinetics of phase change is instantaneous, being driven by the water transport process through the porous network, it can be evaluated either by equations (10) or (11):

$$\overset{\circ}{m}_{\to V} = \rho_L \underline{\nabla}\cdot\left(\frac{\kappa \kappa_r^L}{\eta_L}\left(\frac{R}{M_{H_2O}}\left(\frac{T}{\varphi}\underline{\nabla}\varphi + \ln\varphi\underline{\nabla}T\right) - \frac{\rho_d}{\rho_L}\frac{\partial w_L}{\partial \varphi}\frac{\partial \varphi}{\partial t}\right)\right) \quad (20)$$

$$\overset{\circ}{m}_{\to V} = \frac{\partial m_V}{\partial t} - \underline{\nabla}\cdot\left(D_e^V \frac{M_{H_2O}}{RT}\underline{\nabla}\left(\varphi p_v^{sat}(T)\right)\right) \quad (21)$$

Let us note that, in accordance with the overall mass conservation equation (13), relations (20) and (21) are theoretically equivalent. However, numerical problems can occur depending on which form is used, and the second option requires an evaluation of the term $\partial m_V / \partial t$ which leads to a more complex expression. In [17], this term is simply neglected and only the second term of the right side of eq. (21) is accounted for. It implies to consider the heat source due to phase changes as proportional to the divergence of the water vapor diffusion flow density. A further investigation is needed in order to find the best compromise between a more complicated form or a simpler one but which needs some additional assumptions. In this study, we decide to use the relation (20) to estimate $\overset{\circ}{m}_{\to V}$ because it does not need any assumptions. The influence of this choice on the hygrothermal coupling will be studied in the following. In the end, the injection of (20) in (17) leads to the final form for the heat transfer equation:

$$\rho C_p \frac{\partial T}{\partial t} - \left[L(T,\varphi)\rho_d \frac{\partial w_L}{\partial \varphi} \right] \frac{\partial \varphi}{\partial t} = \underline{\nabla}\cdot\left(\lambda \underline{\nabla} T\right) + L(T,\varphi)\underline{\nabla}\cdot\left({}^{T}_{a}\underline{\nabla} T + {}^{\varphi}_{a}\underline{\nabla}\varphi \right) \quad (22)$$

where

$${}^{T}_{a} = -\rho_L \frac{\kappa \kappa_r^L}{\eta_L} \frac{R}{M_{H_2O}} \ln \varphi \quad (23)$$

$${}^{\varphi}_{a} = -\rho_L \frac{\kappa \kappa_r^L}{\eta_L} \frac{RT}{M_{H_2O}\varphi} \quad (24)$$

Let's note that choosing the other formulation for $m^{\circ}_{\rightarrow V}$, while neglecting $\partial m_V / \partial t$ leads to the following form:

$$\rho C_p \frac{\partial T}{\partial t} = \underline{\nabla}\cdot\left(\lambda \underline{\nabla} T\right) + L(T,\varphi)\underline{\nabla}\cdot\left({}^{T}_{c}\underline{\nabla} T + {}^{\varphi}_{c}\underline{\nabla}\varphi \right) \quad (25)$$

where

$${}^{T}_{c} = \frac{M_{H_2O}}{RT} D_e^V \varphi \frac{dp_v^{sat}(T)}{dT} \quad (26)$$

$${}^{\varphi}_{c} = \frac{M_{H_2O}}{RT} D_e^V p_v^{sat}(T) \quad (27)$$

The influence of the use of eq. (25) instead of eq. (22) is studied in the following section.

3. RESULTS AND DISCUSSION

3.1. Experimental data used for model verification

The model predictions are compared to experimental data for a rammed earth wall of dimensions 1 x1.5x0.3 [m^3]). This wall is instrumented with a water content (Campbell CS616, sensor accuracy of ±2.5 %) and temperature sensor (Campbell CS215, sensor accuracy of ±1.5%), positioned at the central horizontal plane at mid-height (0.5 m high). The experimental design is schematized in **Error! Reference source not found.**a, and is explained more in details in [25]. The wall is placed in a double climatic chamber. Temperature and relative humidity are controlled in one chamber, while their variations in both of them are monitored. The set of experimental condition tested correspond to daily temperature variations between 15 and 20°C within a 50% relative humidity atmosphere (given that the wall is initially saturated).

The material parameters used for the simulations are measured on rammed earth blocks made by the same mason who built the wall, using the same pneumatic rammer and the same manufacturing water content of 19%.

The resulting data and the methods used for the measurements are reported in Table 1 and Table 2 and some additional details are provided in the following paragraphs.

The thermal conductivity was measured on compressed earth blocks (CEB) of 30 x14x10 cm^3 just after their manufacture (when its water content was equal to 19%), and after a drying period of 48 hours, which results in a water content equal to 17%. To ensure the homogeneity of water content within the samples, they were wrapped in a sealed plastic film at least 48 hours at constant temperature before each measurement of thermal conductivity.

The liquid apparent permeability (i.e. $\kappa\kappa_r$) was deduced from the measurement of the A-value (liquid absorption coefficient) as described in [26] and reported in Appendix 4. This formula provides a quite complex variation of the permeability with the water content, which is linearized in the present study for simplification purpose.

Let us eventually note that, as it is already discussed in [27], the manufacturing water content is twice higher than the one normally used in rammed earth [28]. This is due to the presence of 2.5 % by weight of lime NHL5 and the nature of clays.

3.2. Results and model validation against experimental data

The system of partial differential equations (13)-(22) is solved with COMSOL Multiphysics® using PDE module. The simulations are made on a 2D prismatic geometry of length L=0.3m ($\underline{x}$ direction) and height H=1m ($\underline{y}$ direction). It represents a lateral cross section of the tested wall. The finite element mesh used is reported in **Error! Reference source not found.**b (element size of 0.037m) and the time step used is 1s.

Boundary conditions of the simulations are set in accordance with measurements made on both sides of the insulated box. Thus, a null thermal and moisture flow are imposed at the y=0 and y=H boundaries, while thermal and moisture exchanges on the lateral surfaces x=0 and x=L, of normal outward vector n, verify the following equation:

$$\begin{matrix}\left(\underline{g_L}+\underline{g_V}\right)\cdot\underline{n}\\ \underline{g_T}-L\underline{g_L}\cdot\underline{n}\end{matrix}=\begin{matrix}-\rho_L\left(\mathrm{K}^T\underline{\nabla T}+\mathrm{K}^\varphi\underline{\nabla}_\varphi\right)\cdot\underline{n}\\ \left(-\lambda\underline{\nabla T}+L\left(L^T\underline{\nabla T}+L^\varphi\underline{\nabla}_\varphi\right)\right)\cdot\underline{n}\end{matrix}=\begin{matrix}\beta\left(p_v^{sat}\left(T_a\right)\varphi_a-p_v^{sat}\left(T_s\right)\varphi_s\right)\\ \alpha\left(T_a-T_s\right)\end{matrix} \quad (29)$$

where $\underline{n}$ is the outgoing vector at the considered boundary, $\underline{g_L}$ and $\underline{g_V}$ are respectively the liquid water and vapor mass flow vector, $\underline{g_T}$ is the heat flow vector, φ_a and T_a are respectively the relative humidity and temperature of the ambient air while φ_s and T_s are the surface relative humidity and temperature. α [W.m^{-2}.K^{-1}] and β [kg.m^{-2}.s^{-1}.Pa^{-1}] are heat and water vapor transfer coefficients. Let us underline that this boundary condition assumes

not flow of liquid water through the x=0 and x=L surfaces. In other words, all the water which flows to the external surfaces of the wall is assumed to exits in vapor form. The latent effect of this phase change is taken into account by the term $-L\,\underline{g_L}\cdot\underline{n}$ in the boundary condition of the thermal equation.

As suggested by [17], realistic values for β and α are respectively 25.10^{-9} kg.m^{-2}.s^{-1}.Pa^{-1} and 8 W.m^{-2}.K^{-1}. These values will therefore be considered for the following studies.

The water content when just manufactured was around 19%. However, the testing period began after almost one year and a half of drying. At that stage, the water content in the middle of the wall was around to 1,6%, which approximately corresponds to 71% of relative humidity according to its desorption curve. Under this condition, the gaseous phase is connected throughout the wall thickness and vapor transport can occur within the porous network, which is the condition to initiate hygrothermal couplings.

However, this drying period was not sufficient to reach the dynamic equilibrium between the wall and the outside conditions. To take into account this effect, the initial field of temperature and humidity are extracted from the results of a pre-simulation. This latter is realized with the same kind of boundary conditions than (29), i.e. Neumann type, but assuming that T_a and φ_a remain constant and equal to respectively 16°C and 50%, and that the initial temperature and humidity within the wall are homogenous and respectively equal to 20°C and 99%. This pre-calculation stops when the hygrometry at the center of the wall becomes equal to 71%. The temperature and relative humidity profiles can be seen in **Error! Reference source not found.**.

As we are considering a drying phenomenon, the desorption isotherm (Table 2) was used to establish the link between the water content and relative humidity.

Results are reported in **Error! Reference source not found.**, counting measured and simulated data as well as boundary conditions on right and left sides. In terms of temperature, the comparison between measured and simulated distributions in the middle of the wall shows good results. However, as for relative humidity, given the saturated state of the material, the boundary conditions have a few effects on the middle of the wall during the testing time. In addition a small time-laps in temperature is observed between the calculation and the measurements. This may be due to the rough estimation of the thermal capacity of the material. Nevertheless, the simulation and the sensor's data are close.

3.3. Discussion on the model formulation evaluating numerically the impact of different assumptions

The comparison between model predictions and experimental data gives some confidence on the ability of the model to simulate accurately the hygrothermal behavior of rammed earth walls, although it should be kept in mind that, due to experimental limitations, the loading paths considered here remain fairly simple.

To underline the main assets of the coupled model developed in this study and thus to identify the singularity of the hygrothermal behavior of rammed earth, we need to simulate other and more complicated solicitations.

To do so, two numerical experiments, respectively referenced as LP1 and LP2 are considered, with the same geometry but with a width of 50cm, and the same parameters as the one used for the experimental validation. In this cases, the sorption curve (Table 2) was used.

The loading path LP1 considers daily relative humidity sinusoidal cycles between 70% and 50% at a constant temperature of 30°C within the insulated box. The loading path LP2 considers daily temperature cycles between 0°C and 20°C at a constant relative humidity of 60%. Both of the testing periods are set as 100 hours so that the stabilization time in the wall can be observed. A stationary behavior is studied. Let us note that the same boundary conditions are applied on both sides of the wall and that the initial conditions were similar to the boundary conditions in the whole wall. Those two loading paths are summarized in Table 3. For each test conditions, 4 simulations are considered. Each corresponding systems are gathered in Appendix 5.

The first one (referenced as “a”) is based on the system of equations (13)-(22) “as it stands”. The second one (referenced as “b”) considers, like many authors, that the liquid flow is exclusively driven by a relative humidity gradient. The hypothesis 1, on which is based the case “b”, can be written in the form:

$$\text{Case "b"}\left(\text{Hypothesis1}\right): \left| {}^{T}_{1} \right| \ll \left| {}^{T}_{2} \right| \quad (30)$$

where

$${}^{T}_{1} = \left| \frac{\kappa \kappa_r^L}{\eta_L} \frac{\rho_L R}{M_{H_2O}} \ln \varphi \right| ; \quad {}^{T}_{2} = \left| D_e^V \frac{\varphi M_{H_2O}}{\rho_L R T} \frac{dp_V^{sat}(T)}{dT} \right| ; \quad {}^{T}_{1} + {}^{T}_{2} = {}^{T}$$

As previously discussed, the expression of the source term in relative humidity due to temperature variations is thus simplified.

In the third simulation (referenced as “c”), the rate of evaporation/condensation is estimated from eq. (25) under the assumption of negligible variation of vapor mass. The hypothesis 2, on which is based the case “c”, can be written in the form:

$$\text{Case "c"}\left(\text{Hypothesis}\,2\right): MV \ll DD \quad (31)$$

where

$$MV = \left| \frac{\partial m_V}{\partial t} \right| \text{ and } DD = \left| \underline{\nabla} \cdot \left(D_e^V \frac{M_{H_2O}}{RT} \underline{\nabla} \left(\varphi p_v^{sat}(T) \right) \right) \right|$$

Let us note that for cases “a” and “b”, hypothesis are considered independently from one another, i.e. when studying hypothesis 2 (case “b”), the first hypothesis is not made.

At last, in the fourth simulation (referenced as “d”), both of the previous assumption is made. Thus :

$$\text{Case "d" (Hypotheses 1 \& 2)} : \left| \frac{T}{1} \right| \ll \left| \frac{T}{2} \right| \ \& \ MV \ll DD \quad (32)$$

Results of LP1 and LP2 for the four kinds of simulations in temperature and relative humidity are respectively reported in **Error! Reference source not found.** and **Error! Reference source not found.**. Each graph is composed by four curves, corresponding to the four following cases: the complete model (case “a”), model which considers the hypothesis 1 (case “b”), the model which considers the hypothesis 2 (case “c”), and the model which considers hypotheses 1 and 2 (case ”d”).

3.3.1 Effect of the temperature source term on the “relative humidity” equation (hypothesis 1)

The effects of the temperature source term on the “relative humidity” equation can be estimated from the comparison between the simulations “a” and “b”.

Regardless of the loading path considered (either LP1, (**Error! Reference source not found.**) or LP2 (**Error! Reference source not found.**)), the simplification of the source term on the relative humidity equation induced noticeable differences, and especially tends to underestimate the hygrothermal coupling.

Indeed, when LP1 is followed (i.e. hydric cycles), the results reported in Figure 7 show that the hygrothermal effect on temperature due to variation in relative humidity is reduced by about 1.3°C (amplitude of 1.5°C instead of 0.2°C between the complete modeling (“a”) and the one which considers the hypothesis 1 (“b”). The time shift is also impacted as the difference between the two models reaches 0.6 hours (time shift of 7.9 hours for “a” and 7.3 hours for “b”). On the other side, a difference up to 2% is noticeable in terms of relative humidity variations at the middle of the wall.

No significant modifications are observable when we consider the loading path LP2 (**Error! Reference source not found.**, curves “a” and “b”). This result is not surprising since the variations in relative humidity is slight, and thus the hygrothermal coupling remains limited when this leading path is followed.

These results underlines that the impact of thermal gradient on the liquid water transports at constant relative humidity in rammed earth material can be significant. To illustrate this point, the impact of this assumption o the coefficient ^{T} is reported in **Error! Reference source not found.**. Effects are negligible only for high relative humidity and quite high temperatures. However, considering the lifetime solicitations of earth walls, low, and even sub-zero, temperatures and/or relative humidity lower that 60% are not unusual. Let us however underline that, even if strong differences are observed on the coefficient ^{T}, a significant modification of the hygrothermal behavior will occur only if there is a sufficient amount of water within the porous network. Consequently, the necessity to take into account the impact of thermal gradient on liquid pressure at constant humidity is certainly due to the ability of earth materials to keep a non-negligible amount of water, even when the relative humidity decreases below 60%.

3.3.2 Effect of vapor mass variations (hypothesis 2)

In the same way, the effect of the vapor mass variations on the hygrothermal coupling is scanned from the analysis of the simulations “a” and “c”. Results from the LP1’s conditions are different between the complete simulations (“a”) and the ones which consider the hypothesis 2 (“c”). Indeed, we can notice a large difference between the two formulations in terms of amplitude (1.5°C for “a” and 0°C for “c”) while the time shift is not perceptible (7.9hours for “a” and constant for “c”).

On the contrary, not many differences between simulations “a” and “c” arise when the loading path LP2 is considered (i.e. constant imposed φ with temperature cycles). After the transient period, the amplitude in the middle of the wall differs from about 0.7°C (12.7°C for simulation “a” and 12°C for simulation “c” in **Error! Reference source not found.**), while time shift between the solicitations and the response in the middle of the wall is not changed (8 hours for both in **Error! Reference source not found.**).

Actually, let us recall that the simplification of the simulation “c” relies on the assumption that the mass flow of vapor (i.e. $\underline{\nabla}\cdot\left(D_e^V \frac{M_{H_2O}}{RT}\underline{\nabla}\left(\varphi p_v^{sat}(T)\right)\right)$ in eq. (21)) is strongly higher than the overall variation of vapor mass (i.e. $\frac{\partial m_V}{\partial t}$ in eq. (21)), which is due to temperature, vapor pressure and saturation variations. In other terms, the vapor mass income/consumption due to evaporation/condensation processes within a Representative Elementary Volume of the material is instantaneously counterbalanced by the flow of vapor with the adjacent volumes, so that the overall mass of vapor remains constant. This assumption seems quite natural when the flow of water within the porous network of the material is mostly a due to vapor diffusion process (which is the case for most of hygroscopic materials). However, when a significant mass transport of liquid water arises, and/or when strong and fast temperature variations occur, the variation of vapor mass is no longer directly linked to the flow of vapor. Consequently, in function of the external solicitation and of the whole hydric state of the material, the vapor mass variation rate within the pores volumes may become no more negligible towards the flow rate of

vapor mass. Under this condition, in accordance with eq. (21), the hypothesis 2 can induce a bias on the estimation of the evaporation/condensation mass rate ($\overset{\circ}{m}_{\to V}$), and thus on the source term of the thermal equation.

3.3.3. Effect of both hypothesis

To enable to draw a global conclusion on the differences between the complete model and the simplifying assumptions, we made a last case for simulations, considering that both hypothesis 1 and 2 are made (case “d” in **Error! Reference source not found.** and **Error! Reference source not found.**). Globally, we can notice the same effects. In terms of temperature, for the loading path LP1, differences in amplitude are even additive, which leads to even larger differences with the reference simulation “a”. For the loading path LP2, this case “d” is similar to the case “c”, which is based on the hypothesis 2. It is not surprising since the use of the hypothesis 1 was found to have nearly no impact when this loading path is considered.

To conclude on the numerical investigations carried out here, for both cases, extending the simulation duration (to around 1000 hours), a stabilization of the wall is noticed and no difference is remarkable between the different cases. However, on site, no solicitation is applied on such a long period and this scenario is considered unrealistic.

3.3.4 Effects of these hypothesis on moisture and thermal flux

The present paper mainly focuses on material and wall scales. However, this study is part of a larger objective aiming at predicting global exchanges between indoor and outdoor climates through envelops. The link between these two approaches (i.e. material and buildings) can be made through the analysis of the changes induced by the previous hypothesis in terms of moisture and thermal flux at the wall surfaces.

To be clear on the compared quantities, the formulas used are written below, respectively for thermal flux (noted $g_T = \underline{g_T} \cdot \underline{n}$, in W.m^{-2}) and water vapor flux ($g_{RH} = \left(\underline{g_L} + \underline{g_V}\right) \cdot \underline{n}$, in kg.m^{-2}.s^{-1}) at the wall surfaces:

$$g_T = \alpha\left(T_a - T_S\right)\ ;\ g_{RH} = \beta\left(p_V^{sat}\left(T_a\right)\varphi_a - p_V^{sat}\left(T_S\right)\varphi_S\right) \quad (33)$$

with α the heat transfer coefficient, β the moisture transfer coefficient while T_a and T_s are respectively the temperature (in K) of the ambient air and at the surface of the wall, φ_a is the relative humidity of the ambient air, and φ_s is the corresponding value at the surface of the wall.

In order to evaluate the differences between the models in another point of view, Table 4 gathers the maximal heat and moisture flux during the cycles calculated with the different models.

In the case of the hydric cycles (LP1), the absorbed thermal flow at the wall surface is strongly lowered whatever the considered assumption (relative reduction of 72% for the simulation “b” and around 99% for the simulations “c” and “d”). Such high differences are not surprising: indeed, this case has isothermal boundary conditions; therefore heat flux is exclusively due to mass flux. Impact of hypothesis on mass flow is directly seen on heat fluxes. Indeed, the moisture absorption of the wall increases by 26% when the hypothesis 1 is considered, by 18% when the hypothesis 2 is considered and by 37% when both hypotheses are considered.

In addition, it is worth noticing that the order of magnitude of the incomings thermal and moisture flows at the wall surface estimated by the complete model are not negligible (respectively equal to 12.4 W/m² and 1.35. 10^{-5} kg.m^{-2}.s^{-1}). According to this result, if a quite important surface of earth walls is present in a building, it will inevitably impact its thermal and air quality performances.

In the case of LP2, no significant differences are observed between the model “a” and the others, except for the moisture absorption which is increased by 88% if the hypothesis 1 is used. However, the values remain fairly low for this loading path in all the simulations.

Those results are in accordance with the differences observed in terms of temperature and relative humidity in **Error! Reference source not found.** and **Error! Reference source not found.**.

3.3.5 Influence of these hypothesis depending on the income parameters

As it is previously underlined, the hypothesis 1 and 2 are quite common, and, most of the time, they lead to accurate results. The differences observed in this paper are due to the particular transport characteristics of rammed earth material (quite high water content and water permeability in the hygroscopic saturation domain). In order to be more specific on that point, an analysis is performed on the liquid water permeability, which is the transport parameter for which the uncertainty is the most important. Indeed, a direct measurement of the relative permeability in the hygroscopic domain is particularly difficult to realize.

The test is made considering the loading path LP1 as it is the one who leads to the strongest differences between the simulations “a” (reference) and the simulation “d” (accounting for hypothesis 1 and 2).

Since a linear variation of liquid water permeability with water content is considered in the simulation, the parametric study is made on the slope of this latter. The results are presented in **Error! Reference source not found.**. To enable a better understanding, the variation of the liquid permeability with the relative humidity, depending on the slope, are drawn in **Error! Reference source not found.** (a). We chose to compare the models according to the amplitude of the temperature variations at the middle of the wall induced by the hygrothermal coupling.

The comparison between case “a” (complete model) and case “b” (hypothesis 1) is quite intuitive as the permeability is in factor of the additional term. When the permeability is low, the difference between the two formulations tends to zero; as the permeability increases, the gap increases, and can reach 5°C of difference.

It is not surprising that varying the liquid permeability doesn't seem to have any effect when considering the other hypothesis as the hygrothermal coupling are strongly reduced in these cases.

In order to provide an additional illustration of the impact of these hypotheses, the order of magnitude of the ratios $\frac{T}{2}$ / $\frac{T}{1}$ (test of hypothesis 1) and *DD/MV* (test of hypothesis 2) is calculated for each loading path.

The results are illustrated in **Error! Reference source not found.**, which represents, for each hypothesis and each loading path, the variation of the ratios with the diffusion coefficient, for different liquid permeabilities. When the ratio is lower than 10, we consider that the hypothesis is not acceptable. This case is noted as "not valid" in the graphs. However, our simulations show that, when the ratio is lower than 50, noticeable differences are observed between the complete model and the models with the assumptions. This case is noted as "critical" is the graphs. We can observe that, except for a low liquid permeability or a relatively low liquid permeability with high diffusion coefficient, the situation is critical, and both hypotheses 1 and 2 should not be assumed.

4. CONCLUSION

A coupled model, capable of simulating the heat and mass transport, taking into consideration effects due to phase change of water inside the earthen walls, is developed. The main advantage of this model is to consider separately the kinematics of each phase (e.g. liquid water, vapor, dry air and solid matrix), in interaction with each other. It also accounts for the impact of pore water pressure on the liquid-to-vapor phase change, and hence on the resulting latent heat released or absorbed.

The comparison with experimental data on a metric rammed earth wall underlines the ability of the model to reproduce properly the hygrothermal behavior of this material.

Afterward, the model is used to assess the accuracy and impacts of the simplifying assumptions commonly made by the hygrothermal models for buildings materials. It follows that, due the particularities the material (from very low water content to near saturation, high porosity, large variation of water content during its life-time, …), it is necessary to take into account the impact of thermal gradient on water flow and the variation of in-pore vapor mass due to evaporation-condensation. However, the sensibility analysis realized on the liquid water permeability underlines that these simplifying assumptions can be made for materials with a sufficiently low water permeability, which is the case for most hygroscopic materials.

ACKNOWLEDGMENTS

I would like to thank Stephane Cointet and Nicolas Meunier for the earth supply and their technical support.
The present work has been supported by the French Research National Agency (ANR) through the “Villes et Bâtiments Durables” program (Project Primaterre n°. ANR-12-VBDU-0001).

This work is also cofounded by the French Environmental agency ADEME, Lafarge (TEZ10-44), the Région Rhône-Alpes (11024835 01 – ENT012v de la Direction du Climat, Environnement, Santé et Énergie, and a Fellowship CMIRA for JC Morel).

Finally, we thank the anonymous reviewers for their detailed reviews of an earlier version of this article, which led to significant improvements.

APPENDIX 1

Let’s consider for this part the pure phase I. Its specific free enthalpy reads[24]:

$$dG_I = \phi_I dp_I - S_I dT + \mu_I dn_I \quad \text{(A1.1)}$$

where μ_I is the chemical potential of I, S_I and n_I are the entropy and the mole quantity of I per unit of porous media.
Moreover, the following equations of states can be derived from the well-known Gibbs-Duhem relation:

$$\frac{1}{\rho_I} = \frac{\partial g_I}{\partial p_I} \; ; s_I = -\frac{\partial g_I}{\partial T} \quad \text{(A1.2)}$$

Assuming the liquid water is a pure phase, equations (A1) and (A2) can be applied. Linking the free enthalpy to the chemical potential through the Euler relation, under the small perturbations assumption, and keeping only the first order terms, the integration of the equations of states leads to:

$$g_L = g_L^0 - s_L^0 \left(T - T_0\right) - C_{p,L} \left[T \ln \left[\frac{T}{T_0} \right] - \left(T - T_0\right) \right] + \frac{p_L}{\rho_L} \quad \text{(A1.3)}$$

Assuming the phase G as an ideal gas mixture of perfect gas and estimating the specific free enthalpy of the water vapor from its standard specific free enthalpy, to whom equations (A1) and (A2) can be applied, the specific free enthalpy of the water vapor reads:

$$g_V = g_V^0 - s_V^0 \left(T - T_0\right) - C_{p,V} \left[T \ln \left[\frac{T}{T_0} \right] - \left(T - T_0\right) \right] + \frac{RT}{M_{H_2O}} \ln \left[\frac{p_V}{p_V^0} \right] \quad \text{(A1.4)}$$

Through equation (A1.2), specific free entropy of liquid water and water vapor can be estimated, at first order, by:

$$s_L = s_L^0 + C_{p,L} \ln \left[\frac{T}{T_0} \right] \quad \text{(A1.5)}$$

$$s_V = s_V^0 + C_{p,V} \ln \left[\frac{T}{T_0} \right] - \frac{R}{M_{H_2O}} \ln \left[\frac{p_V}{p_V^{sat}\left(T_0\right)} \right] \quad \text{(A1.6)}$$

Finally, the integral enthalpy associated to the liquid to vapor phase change, defined as $L = T\left(s_V - s_L\right)$ (see [29], for example) is a function of the temperature and the equilibrium vapor pressure. Using equations (5)(A1.3)(A1.5)(A1.6), this expression eventually becomes:

$$\boxed{L = L_0 + \left(C_{p,V} - C_{p,L}\right)\left(T - T_0\right) - \frac{RT}{M_{H_2O}} \ln \varphi} \quad \text{(A1.7)}$$

Another way to derive this relation is to use the following Clausius-Clapeyron-like relation:

$$L = -\frac{R}{M_w} \frac{\partial ln\left(p_V\right)}{\partial\left(1/T\right)}\bigg|_{p_L} = \frac{RT^2}{M_w} \frac{\partial ln\left(p_V\right)}{\partial T}\bigg|_{p_L} \quad \textbf{(A1.13)}$$

Since $\boldsymbol{p_V = \varphi\, p_V^{sat}}$, the use of the Kelvin's law (4) allows to write this equation in the following form:

$$L = -\frac{RT}{M_w} \ln\left(\varphi\right) + \frac{RT^2}{M_w p_V^{sat}} \frac{dp_V^{sat}}{dT} \quad \textbf{(A1.16)}$$

The final step consists in replacing $\boldsymbol{p_V^{sat}}$ by its expression reported in eq. (6). It leads to:

$$\frac{dp_V^{sat}}{dT} = \frac{M_w}{RT^2}\, p_V^{sat} \left(L_0 + \left(C_{p,1} - C_{p,2}\right)\left(T - T_0\right)\right) \quad \textbf{(A1.18)}$$

which eventually gives:

$$\boxed{L = L_0 + \left(C_{p,1} - C_{p,2}\right)\left(T - T_0\right) - \frac{RT}{M_w}\ln\left(\varphi\right)} \textbf{(A1.19)}$$

APPENDIX 2

According to the second law of thermodynamics and assuming no source volume term of heat, the entropy balance is equal to:

$$\frac{\partial S}{\partial t} + \underline{\nabla} \cdot \sum_{i=L,V,A} s_i m_i \underline{V_i} = -\underline{\nabla} \cdot \frac{\underline{q}}{T} + \frac{D}{T} \text{ (A2.1)}$$

where:

- S is the total entropy of the porous medium, equal to the sum of the entropy of each phase: $S = S_s + m_L S_L + m_A S_A + m_V S_V$
- $\underline{q}$ is the outgoing heat flow vector that follows the Fourier Law : $\underline{q} = -\lambda \underline{\nabla} T$
- D stands for the total dissipation of the system, equal to the sum of the mechanical dissipation D_M of the skeleton and the in-pore fluids, and the thermal dissipation D_{th} The latter is equal to:

$$D_{th} = -\frac{\underline{q}}{T} \underline{\nabla} T \text{ (A2.2)}$$

The combination of all this leads to:

$$T\frac{\partial S}{\partial t}+T\sum_i s_i\underline{\nabla}\cdot\left(m_i\underline{V}_i\right)+\sum_i\left(m_i\underline{V}_i\right)\underline{\nabla s_i}=-T\left(\frac{1}{T}\underline{\nabla}\cdot\underline{q}-\underline{\nabla}\left(\frac{1}{T}\right)\cdot\underline{q}+\underline{q}\frac{\underline{\nabla}T}{T}\right)+D_M \quad \text{(A2.3)}$$

In the following, we consider the heat source due to mechanical dissipation is negligible. Under these assumptions, accounting for the mass conservation equations and the previous equations, it becomes:

$$T\left(\frac{\partial S_S}{\partial t}+\sum_{i=L,V,A}m_i\frac{\partial s_i}{\partial t}+\dot{m}_{\to V}\left(s_V-s_L\right)\right)+\sum_{i=L,V,A}\underline{g_i}\cdot\underline{\nabla s_i}=-\underline{\nabla}\cdot\underline{q} \quad \text{(A2.4)}$$

Where $\underline{g_i}=m_i\underline{V_i}$ is the mass filtration vector of the phase *i*. Assuming that the entropy of the solid skeleton is only function of temperature, it reads:

$$\mathrm{d}S_S=\left(1-\phi\right)\rho_S\frac{C_S}{T} \quad \text{(A2.5)}$$

where C_S is the specific heat at constant pressure of the solid skeleton. On the other side, the use of the state functions combined with the specific free enthalpy expressions leads, at first order, to:

$$\mathrm{d}s_L = \frac{C_L}{T}\mathrm{d}T \text{ and } ds_V = \frac{C_V}{T}\mathrm{d}T \quad \text{(A2.6)}$$

The use of these three last relations and of the expression of the integral enthalpy of evaporation $L = T\left(s_V - s_L\right)$ leads to the following expression:

$$\rho C_p \frac{\partial T}{\partial t} + \sum_{i=L,V,A} C_i \underline{g_i} \cdot \underline{\nabla T} + m^{\circ}_{\rightarrow V} L\left(T,\varphi\right) = \underline{\nabla}\cdot\left(\lambda \underline{\nabla}\mathrm{T}\right) \quad \text{(A2.7)}$$

where $\rho C_p = \left(1-\phi\right)\rho_S C_{p,S} + \phi S_r \rho_L C_{p,L} + \phi\left(1-S_r\right)\left(\rho_A C_{p,A} + \rho_V C_{p,V}\right)$ is the average heat capacity at constant pressure. This equation allows to clearly identifying the different terms of the heat balance. The term $(\underline{\nabla}\cdot\left(\lambda \underline{\nabla}\mathrm{T}\right))$ stands for the heat flow, which is equal to the sum of the variation in sensitive heat $(\rho C_p \frac{\partial T}{\partial t} + \sum_{i=L,V,A} C_i \underline{g_i} \cdot \underline{\nabla T})$ (which becomes null if the temperature is constant and homogeneous) and in latent heat $(m^{\circ}_{\rightarrow V} L\left(T,\varphi\right))$ (which becomes null if there is no liquid to vapor phase change). The second term of the sensitive heat variation, namely $\sum_{i=L,V,A} C_i \underline{g_i} \cdot \underline{\nabla T}$, is due to the heat convectively transported by the fluids (vapor and water). This term can be neglected when the Péclet number is strongly lower than 1, which is the case for heat transfer within earth material (because $\lambda \gg \sum_{i=L,V,A} C_i \underline{g_i} l$, where l is the characteristic length of the considered system). This assumption allows then to write the thermal equation in its final form:

$$\rho C_p \frac{\partial T}{\partial t} = \underline{\nabla}\cdot\left(\lambda \underline{\nabla} \mathrm{T}\right) - \overset{\circ}{m}_{\to V} L\left(T, \varphi\right) \text{(A2.8)}$$

APPENDIX 3

Usually considered as a reference and implemented in the software WUFI, the formulation detailed in [17] leads to characteristic parameters. In order to ensure the right understanding of the formulation presented in this paper, the connection between the coefficients is highlighted in this appendix.

The final formulation of the coupled equations in [17] reads :

$$\frac{\partial H}{\partial T}\frac{\partial T}{\partial t} = \underline{\nabla}\cdot\left(\lambda \nabla T\right) + h_v \underline{\nabla}\cdot\left(\delta_p \nabla\left(\varphi \mathrm{p}_{\mathrm{sat}}\right)\right) \textbf{(A3.1)}$$

$$\frac{\partial w_p}{\partial \varphi}\frac{\partial \varphi}{\partial t} = \underline{\nabla}\cdot\left(\mathrm{D}_{\varphi} \nabla \varphi + \delta_{\mathrm{p}} \nabla\left(\varphi \mathrm{p}_{\mathrm{sat}}\right)\right) \textbf{(A3.2)}$$

With $\boldsymbol{w_p}$ the water content in kg.m^{-3}.

Taking into account the hypothesis already mentioned in the article, and given equations (12) and (21), we finally obtain:

$$h_v = L\left(\varphi, T\right) \textbf{(A3.3)}$$

$$D_\varphi = \rho_L^2 \frac{\kappa \kappa_r^L}{\eta_L} \frac{RT}{M_{H_2O} \varphi} \quad \textbf{(A3.4)}$$

$$\delta_p = D_e^V \frac{M_{H_2O}}{RT} \quad \textbf{(A3.5)}$$

APPENDIX 4: ESTIMATION OF THE PERMEABILITY

The global liquid permeability of a material depends on the amount of water present in the pores. We thus consider a variation of $\boldsymbol{\kappa \kappa_r^L}$ with the water content as advised in [26], given by the following formula :

(A4.1)

where $\boldsymbol{D_{ws}}$ is the capillary transport coefficient, $\boldsymbol{A}$ the water absorption coefficient and $\boldsymbol{\omega_f}$ the free water saturation in kg.m^{-3}. As illustrated in the Appendix 3, a link exist between the coefficient $\boldsymbol{D_\varphi}$, and thus $\boldsymbol{D_{ws}}$, and the income parameters of our formulation which enables us to deduce a water content dependent expression of the liquid permeability :

$$\kappa \kappa_r^L = \frac{M_{H_2O} \varphi}{RT} \frac{\eta_L}{\rho_L^2} D_{ws} \frac{\partial \omega}{\partial \varphi} \quad \textbf{(A4.2)}$$

where $\frac{\partial \omega}{\partial \varphi}$ is the slope of the sorption isotherm.

For numerical simplification purpose, we then chose to consider a linear variation of the liquid permeability with the water content, within the same boundaries. The variation of the liquid permeability with the relative humidity as defined previously is represented in Figure 10(a) (“original”), among the linear variations used for the parametric study (named by their slope).

We thus have the relation:

$$\kappa\kappa_r^L = k\,\omega \quad \textbf{(A4.3)}$$

where $\boldsymbol{k}$ is the slope of the linear approximation.

APPENDIX 5: SYSTEMS CORRESPONDING TO THE DIFFERENT HYPOTHESIS

The four simulations carried out in part 3.3 consider four different system of equation, coming from hypothesis explained previously. To make things clearer, those four systems are gathered in the appendix.

4.a Complete model

The first one considers none of the hypotheses, and is referenced as “a”.

$$\frac{1}{\rho_L}\left(\rho_d \frac{\partial w_L}{\partial \varphi} + \phi_G \frac{M_{H_2O}\, p_v^{sat}(T)}{RT}\right)\frac{\partial \varphi}{\partial t} + \frac{\phi_G \rho_V^{\alpha}}{\rho_L}\frac{\partial T}{\partial t} = \nabla\cdot\left(\lambda_a^T \nabla T + \delta_a^{\varphi}\nabla\varphi\right) \quad \text{(A4.1)}$$

$$\rho_V^{\alpha} = \varphi \frac{p_V^{sat}(T) M_{H_2O}}{RT}\left(\frac{1}{p_V^{sat}(T)}\frac{dp_V^{sat}(T)}{dT} - \frac{1}{T}\right) \quad \text{(A4.2)}$$

$$\lambda_a^T = \lambda_1^T + \lambda_2^T = \frac{\kappa\kappa_r^L}{\eta_L}\frac{\rho_L R}{M_{H_2O}}\ln\varphi + D_e^V \frac{\varphi M_{H_2O}}{\rho_L RT}\frac{dp_V^{sat}(T)}{dT} \quad \text{(A4.3)}$$

$$\overset{\varphi}{a} = \frac{\kappa\kappa_r^L}{\eta_L}\frac{\rho_L RT}{M_{H_2O}\varphi} + D_e^V \frac{M_{H_2O}}{\rho_L RT} p_V^{sat}(T) \quad \text{(A4.4)}$$

$$\rho C_p \frac{\partial T}{\partial t} - \quad L(T,\varphi)\rho_d \frac{\partial w_L}{\partial \varphi} \quad \frac{\partial \varphi}{\partial t} = \underline{\nabla}\cdot\left(\lambda \underline{\nabla} T\right) + L(T,\varphi)\underline{\nabla}\cdot\left(\quad {}^{T}\underline{\nabla} T + \quad {}^{\varphi}\underline{\nabla}\varphi\right) \quad \text{(A4.5)}$$

$$\overset{T}{a} = -\rho_L \frac{\kappa\kappa_r^L}{\eta_L}\frac{R}{M_{H_2O}} \ln\varphi \quad \text{(A4.6)}$$

$$\overset{\varphi}{a} = -\rho_L \frac{\kappa\kappa_r^L}{\eta_L}\frac{RT}{M_{H_2O}\varphi} \quad \text{(A4.7)}$$

4.b Model with hypothesis 1

The second one considers only the hypothesis 1 related to the flow of liquid water, and is referenced as “b”.

$$\frac{1}{\rho_L} \quad \rho_d \frac{\partial w_L}{\partial \varphi} + \phi_G \frac{M_{H_2O} p_v^{sat}(T)}{RT} \quad \frac{\partial \varphi}{\partial t} + \frac{\phi_G \rho_V^{\alpha}}{\rho_L}\frac{\partial T}{\partial t} = \underline{\nabla}\cdot\left(\quad {}^{T}\underline{\nabla} T + \quad {}^{\varphi}\underline{\nabla}\varphi\right) \quad \text{(A4.1)}$$

$$\rho_V^{\alpha} = \varphi \frac{p_V^{sat}(T) M_{H_2O}}{RT} \quad \frac{1}{p_V^{sat}(T)}\frac{dp_V^{sat}(T)}{dT} - \frac{1}{T} \quad \text{(A4.2)}$$

$$\overset{T}{b} = \quad \overset{T}{2} = D_e^V \frac{\varphi M_{H_2O}}{\rho_L RT}\frac{dp_V^{sat}(T)}{dT} \quad \text{(A4.8)}$$

$$\overset{\varphi}{a} = \frac{\kappa\kappa_r^L}{\eta_L}\frac{\rho_L RT}{M_{H_2O}\varphi} + D_e^V \frac{M_{H_2O}}{\rho_L RT} p_V^{sat}(T) \quad \text{(A4.4)}$$

$$\rho C_p \frac{\partial T}{\partial t} - L(T,\varphi)\rho_d \frac{\partial w_L}{\partial \varphi}\frac{\partial \varphi}{\partial t} = \underline{\nabla}\cdot\left(\lambda \underline{\nabla} T\right) + L(T,\varphi)\underline{\nabla}\cdot\left({}^{T}\underline{\nabla} T + {}^{\varphi}\underline{\nabla}\varphi\right) \quad \text{(A4.5)}$$

$${}^{T}_{a} = -\rho_L \frac{\kappa \kappa_r^L}{\eta_L}\frac{R}{M_{H_2O}} \ln\varphi \quad \text{(A4.6)}$$

$${}^{\varphi}_{a} = -\rho_L \frac{\kappa \kappa_r^L}{\eta_L}\frac{RT}{M_{H_2O}\varphi} \quad \text{(A4.7)}$$

4.c Model with hypothesis 2

The third one considers only the hypothesis 2 related to the expression of the evaporation / condensation rate, and is referenced as “c”.

$$\frac{1}{\rho_L}\rho_d \frac{\partial w_L}{\partial \varphi} + \phi_G \frac{M_{H_2O} p_v^{sat}(T)}{RT}\frac{\partial \varphi}{\partial t} + \frac{\phi_G \rho_V^{\alpha}}{\rho_L}\frac{\partial T}{\partial t} = \underline{\nabla}\cdot\left({}^{T}\underline{\nabla} T + {}^{\varphi}\underline{\nabla}\varphi\right) \quad \text{(A4.1)}$$

$$\rho_V^{\alpha} = \varphi \frac{p_V^{sat}(T) M_{H_2O}}{RT}\left(\frac{1}{p_V^{sat}(T)}\frac{dp_V^{sat}(T)}{dT} - \frac{1}{T}\right) \quad \text{(A4.2)}$$

$${}^{T}_{a} = {}^{T}_{1} + {}^{T}_{2} = \frac{\kappa \kappa_r^L}{\eta_L}\frac{\rho_L R}{M_{H_2O}} \ln\varphi + D_e^V \frac{\varphi M_{H_2O}}{\rho_L RT}\frac{dp_V^{sat}(T)}{dT} \quad \text{(A4.3)}$$

$${}^{\varphi}_{a} = \frac{\kappa \kappa_r^L}{\eta_L}\frac{\rho_L RT}{M_{H_2O}\varphi} + D_e^V \frac{M_{H_2O}}{\rho_L RT} p_V^{sat}(T) \quad \text{(A4.4)}$$

$$\rho C_p \frac{\partial T}{\partial t} = \underline{\nabla}\cdot\left(\lambda \underline{\nabla} T\right) + L\left(T,\varphi\right)\underline{\nabla}\cdot\left(\quad {}^{T}\underline{\nabla} T + \quad {}^{\varphi}\underline{\nabla}\varphi\right) \text{(A4.9)}$$

$${}^{T}_{c} = \frac{M_{H_2O}}{RT} D_e^V \varphi \frac{dp_v^{sat}\left(T\right)}{dT} \text{(A4.10)}$$

$${}^{\varphi}_{c} = \frac{M_{H_2O}}{RT} D_e^V p_v^{sat}\left(T\right) \text{(A4.11)}$$

4.d Model with hypothesis 1 + 2

The last and fourth one considers both the hypothesis 1 and 2, and is referenced as “d”.

$$\frac{1}{\rho_L} \rho_d \frac{\partial w_L}{\partial \varphi} + \phi_G \frac{M_{H_2O} p_v^{sat}\left(T\right)}{RT} \frac{\partial \varphi}{\partial t} + \frac{\phi_G \rho_V^{\alpha}}{\rho_L} \frac{\partial T}{\partial t} = \underline{\nabla}\cdot\left(\quad {}^{T}\underline{\nabla} T + \quad {}^{\varphi}\underline{\nabla}\varphi\right) \text{(A4.1)}$$

$$\rho_V^{\alpha} = \varphi \frac{p_V^{sat}\left(T\right) M_{H_2O}}{RT} \frac{1}{p_V^{sat}\left(T\right)} \frac{dp_V^{sat}\left(T\right)}{dT} - \frac{1}{T} \quad \text{(A4.2)}$$

$${}^{T}_{b} = {}^{T}_{2} = D_e^V \frac{\varphi M_{H_2O}}{\rho_L RT} \frac{dp_V^{sat}\left(T\right)}{dT} \text{(A4.8)}$$

$${}^{\varphi}_{a} = \frac{\kappa \kappa_r^L}{\eta_L} \frac{\rho_L RT}{M_{H_2O}\varphi} + D_e^V \frac{M_{H_2O}}{\rho_L RT} p_V^{sat}\left(T\right) \text{(A4.4)}$$

$$\rho C_p \frac{\partial T}{\partial t} = \underline{\nabla}\cdot\left(\lambda \underline{\nabla} T\right) + L\left(T,\varphi\right)\underline{\nabla}\cdot\left(\quad {}^{T}\underline{\nabla} T + \quad {}^{\varphi}\underline{\nabla}\varphi\right) \text{(A4.9)}$$

$${}^{T}_{c} = \frac{M_{H_2O}}{RT} D_e^V \varphi \frac{dp_v^{sat}\left(T\right)}{dT} \text{(A4.10)}$$

$$\varphi_c = \frac{M_{H_2O}}{RT} D_e^V p_v^{sat}(T) \quad \text{(A4.11)}$$

REFERENCES

[1] M. K. Dixit, J. Fernandez-Solis, S. Lavy, and C. H. Culp, “Identification of parameters for embodied energy measurement: A literature review,” *Energy Build.*, no. 42, pp. 1238–1247, 2010.

[2] D. J. Harris, “A quantitative approach to the assessment of the environmental impact of building materials,” *Build. Environ.*, vol. 34, pp. 751–758, 1999.

[3] S. H. Sameh, “Promoting earth architecture as a sustainable construction technique in Egypt,” *J. Clean. Prod.*, pp. 1–12, 2013.

[4] G. Habert, E. Castillo, E. Vincens, and J. Morel, “Power: A new paradigm for energy use in sustainable construction,” *Ecol. Indic.*, vol. 23, pp. 109–115.

[5] S. Liuzzi, M. R. Hall, P. Stefanizzi, and S. P. Casey, “Hygrothermal behaviour and relative humidity buffering of unfired and hydrated lime-stabilised clay composites in a Mediterranean climate,” *Build. Environ.*, vol. 61, pp. 82–92, 2013.

[6] F. McGregor, A. Heath, E. Fodde, and A. Shea, “Conditions affecting the moisture buffering measurement performed on Compressed Earth Blocks,” *Build. Environ.*, 2013.

[7] E. P. Barrett, L. G. Joyner, and P. . Halenda, “The determination of pore volume and area distributions in porous substances. I. Computations from nitrogen isotherms,” *J. Am. Chem. Soc.*, vol. 73, pp. 373–380, 1951.

[8] M. Hall and D. Allinson, “Assessing the effects of soil grading on the moisture content-dependent thermal conductivity of stabilised rammed earth materials,” *Appl. Therm. Eng.*, vol. 29, pp. 740–747, 2009.

[9] T. . Desta, J. Langmans, and S. Roels, “Experimental data set for validation of heat, air and moisture transport models of building envelopes,” *Build. Environ.*, vol. 46, pp. 1038–1046, 2011.

[10] K. Abahri, R. Belarbi, and A. Trabelsi, “Contribution to analytical and numerical study of combined heat and moisture transfers in porous building materials,” *Build. Environ.*, vol. 46, pp. 1354–1360, 2011.

[11] D. Allinson and M. R. Hall, “Hygrothermal analysis of a stabilised rammed earth test building in the UK,” *Energy Build.*, vol. 42, pp. 845–852, 2010.

[12] M. Hall and D. Allinson, “Transient numerical and physical modelling of temperature profile evolution in stabilised rammed earth walls,” *Appl. Therm. Eng.*, vol. 30, pp. 433–441, 2010.

[13] F. Collet, “Study of the thermal behaviour of clay walls facing south,” *Build. Environ.*, vol. 41, pp. 307–315, 2006.

[14] S. Whitaker, *Simultaneous Heat, Mass, and Momentum Transfer in Porous Media: A Theory of Drying*, vol. 13. 1977, pp. 119–203.

[15] W. Gray, “General conservation equations for multi-phase systems,” *Adv. Water Resour.*, vol. 6, pp. 130–140, 1983.

[16] J. R. Philip and D. . De Vries, “Moisture movement in porous materials under temperature gradients,” *Trans. Am. Geophys. Union*, vol. 38, pp. 222–232, 1957.

[17] H. M. Künzel, “Simultaneous heat and moisture transport in building components one - and two-dimensional calculation using simple parameters - Report on PhD thesis, Fraunhofer Institute of Building Physics,” 1995.

[18] A. V. Luikov, “Systems of differential equations of heat and mass transfer in capillary-porous bodies,” *Int. J. Heat Mass Transf.*, vol. 18, no. Pergamon Press, pp. 1–14, 1975.

[19] Fraunhofer, “IBP / WUFI.” [Online]. Available: http://www.wufi.de/. [Accessed: 08-Feb-2013].

[20] J. Grünewald, “Diffusiver und Konvektiver Stoff-und Energietransport in kapillarporösen Baustoffen,” Technische Universität Dresden, Germany, 1997.

[21] O. Coussy, *Poromechanics*. 2004, p. 312.

[22] H. Janssen, “Thermal diffusion of water vapour in porous materials: Fact or fiction?,” *Int. J. Heat Mass Transf.*, vol. 54, pp. 1548–1562, Mar. 2011.

[23] A. Fabbri, O. Coussy, T. Fen-Chong, and P. Monteiro, “Are deicing salt necessary to promote scaling in concrete?,” *J. Eng. Mech.*, vol. 134, pp. 589–598, 2008.

[24] D. Kondepudi and I. Prigogine, *Modern Thermodynamics: From the Heat Engines to Dissipative Structures*, John Wiley. 1998.

[25] P.-A. Chabriac, A. Fabbri, J. C. Morel, J.-P. Laurent, and J. Blanc-Gonnet, “A procedure to measure the in-situ water content in rammed earth and cob,” *Materials (Basel).*, vol. 7, pp. 3002–3020, 2014.

[26] K. Kießl, “Capillary and vaporous moisture transport in multi-layered building components,” Universität-Gesamthochschule Essen, 1983.

[27] P.-A. Chabriac, “Mesure du comportement hygrothermique du pisé,” ENTPE, Université de Lyon, France, 2014.

[28] Q. B. Bui and J. Morel, “Assessing the anisotropy of rammed earth,” *Constr. Build. Mater.*, vol. 23, pp. 3005–3011, 2009.

[29] F. Rouquerol, J. Rouquerol and K. Sing, "Adsorption by Powders and Porous Solids" Academic press, 467p, 1999

Fig. 1 Schematic representation of the heat and water transfers within an earth wall. φ stands for the relative humidity, T for the temperature and p_V^{sat} for the equilibrium vapor pressure.

Fig. 2 Schematic representation of the different phases considered in the model and their interactions.

Fig. 3 (a): Calculated and tabulated values of $L(T)$. **(b)** : Evolution of L with the equilibrium relative humidity at different temperatures.

Fig. 4 (a) Photography and schematic representation of the model wall ; (b) Geometry and spatial discretization of the 50cm and 30cm walls

Fig. 5 Temperature and relative humidity profiles in the wall after the pre-calculation

Fig. 6 Comparison between measured and simulated temperature distributions in the middle of the wall (Point A) with boundary conditions on the right (BC_r) and left (BC_l) sides, for 3 weeks and for 24 hours

Fig. 7 Simulations results of LP1 for the different formulations.

Fig. 8 Simulations results of LP2 for the different formulations

Fig. 9 (a): Ratio of the two terms in ^{T} against relative humidity for different T. **(b)** : Ratio of the two terms in ^{T} against T for different relative humidity

Fig. 10 (a) Variation of the liquid permeability with the relative humidity, depending on the slope of the linear variation with water content **(b)** Influence of the liquid permeability (taken at 50%RH) on the hygrothermal coupling effects (amplitude **(a)**) depending on the hypothesis when following LP1

Fig. 11 Variation of the ratio between the coefficient kept and the one neglected for different values of liquid permeabilities and coefficient diffusion, for both loading paths and hypothesis

Table 1 Input parameters used for the simulations.

Parameters	Value	Experimental method
ρ_d	1730±40 [kg.m^{-3}]	Hydrostatic weighing
ϕ	0.35	$\phi = 1 - \frac{\rho_d}{\rho_g}$ where ρ_g = 2650kg.m^{-3} according to [6]
D_e^V	2.70e-6 [m^2.s^{-1}]	Dry cup method after NF EN ISO 12572:2001
A	0.39 [kg.m^{-2}.s$^{-1/2}$]	According to EN 1015-18
ω_f	259 [kg.m^{-3}]	According to the A-value measured following [26]
$\kappa\kappa_r^l$	10^{-18} [illegible]w [m²]	Deduced from the A-value according to [26]
$C_{p,S}$	648 [J.kg^{-1}.K^{-1}]	Differential Scanning Calorimetry (DSC)
$\lambda(w=0\%)$ $\lambda(w=17\%)$	0.6 [W.m^{-1}.K^{-1}] 2.1 [W.m^{-1}.K^{-1}] 2.4 [W.m^{-1}.K^{-1}]	Hot wire apparatus, measured on a CEB just after manufacturing (19%), after 48h drying (17%) and totally dried (0%)

$\lambda(w=19\%)$		

Table 2 Sorption and desorption isotherms at 20°C of the studied material

Relative humidity [-]	Water content [mass%]	Experimental method
$\varphi = 0$	0	NF EN ISO 12571:2000
$\varphi = 0.23$ $\varphi = 0.43$	0.3	
$\varphi = 0.59$	0.5	
$\varphi = 0.76$	0.7	
$\varphi = 0.86$	1.3	
$\varphi = 0.97$	1.6	
$\varphi = 0.99$	6.1	
	10	
$\varphi = 0$	0	NF EN ISO 12571:2000
$\varphi = 0.43$	0.8	
$\varphi = 0.59$	1.2	
$\varphi = 0.76$	1.9	
$\varphi = 0.86$	2.6	
$\varphi = 0.97$	7.3	
$\varphi = 0.99$	19.9	

Table 3 Loading paths LP1 and LP2.

		LP1	LP2
Boundary conditions	RH	daily cycles 70-50%	60%
	T	30°C	daily cycles 0-20°C
Initial conditions	RH	70%	60%
	T	30°C	0°C

Figure 1

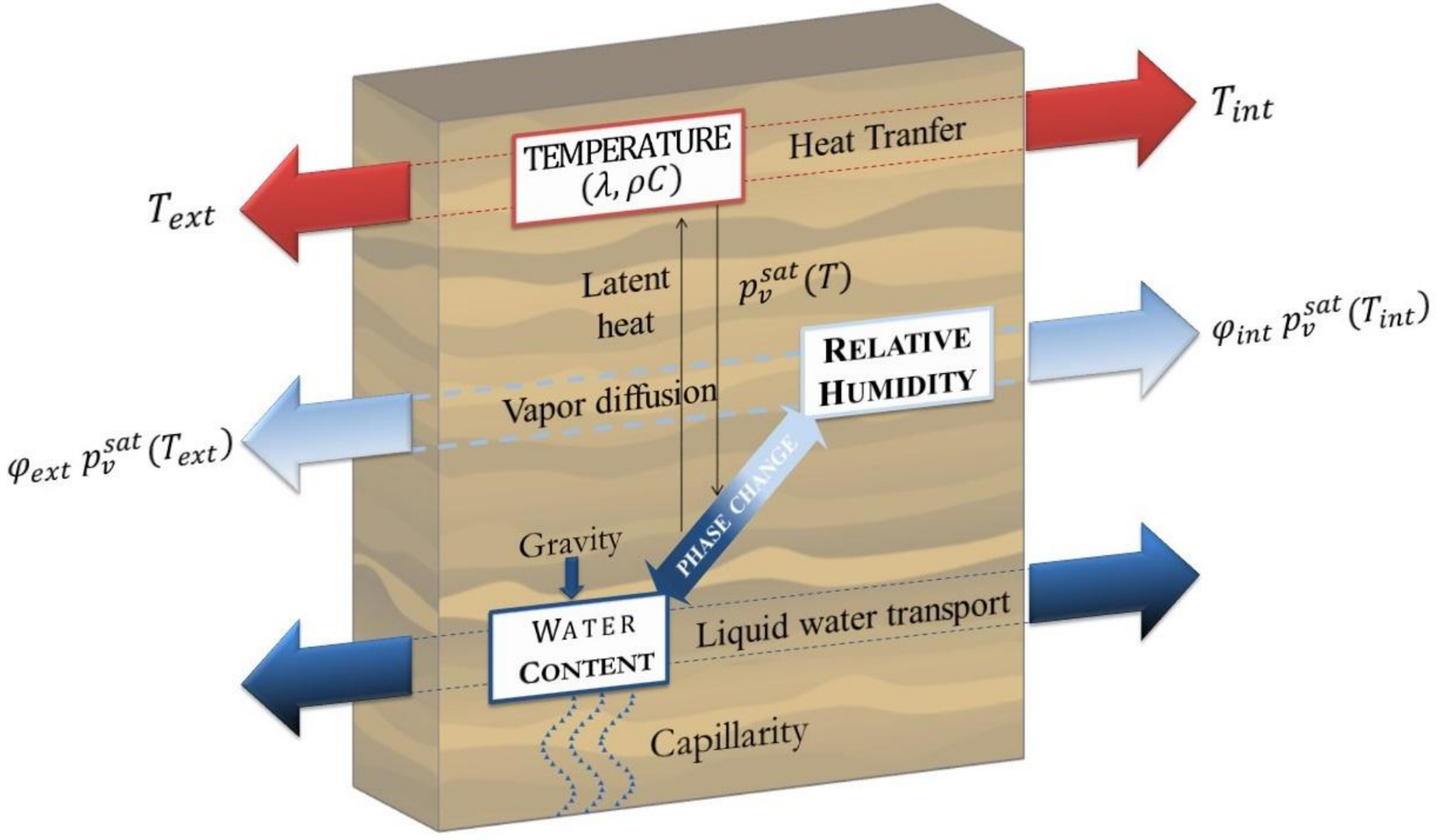

Figure 2

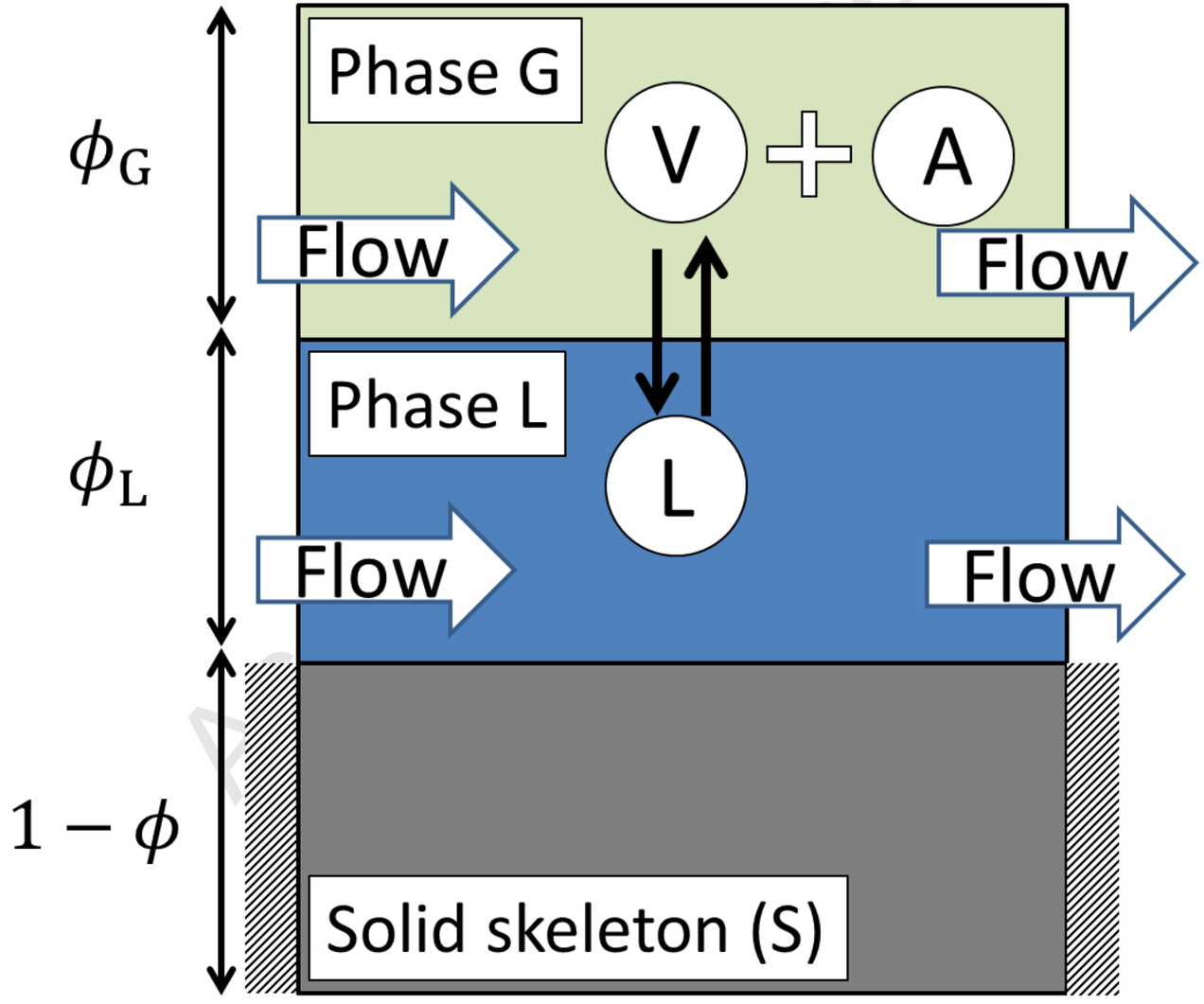

Figure 3

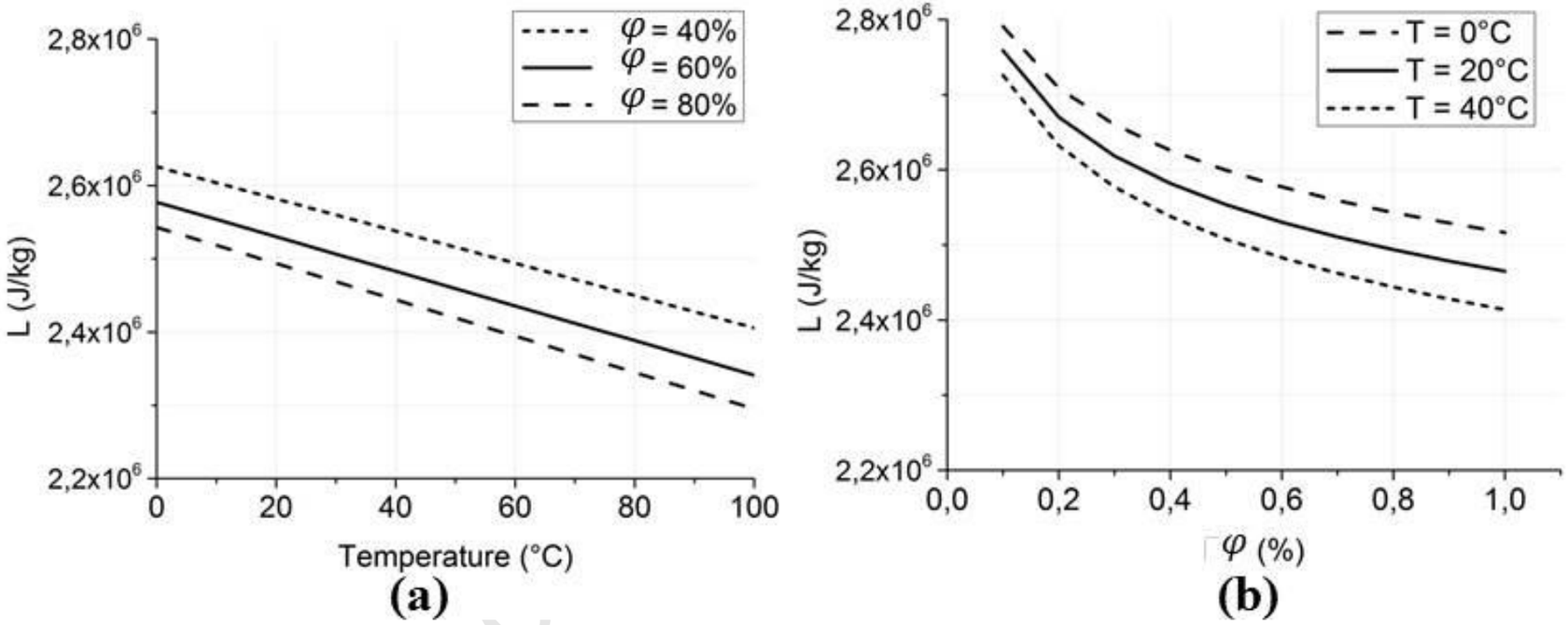

Figure 4

(a)

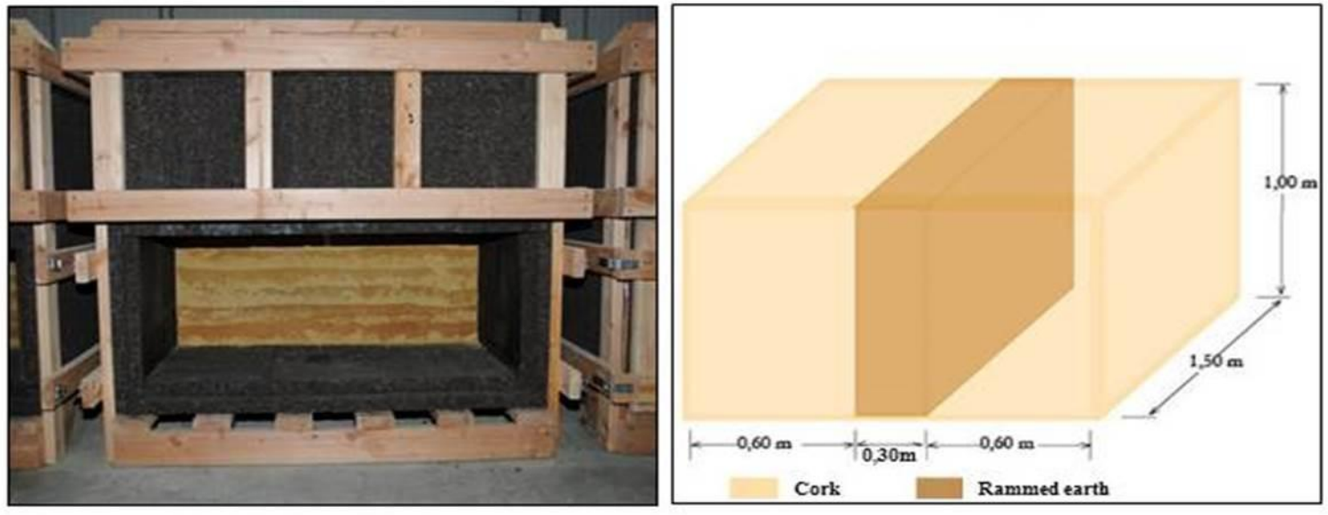

(b)

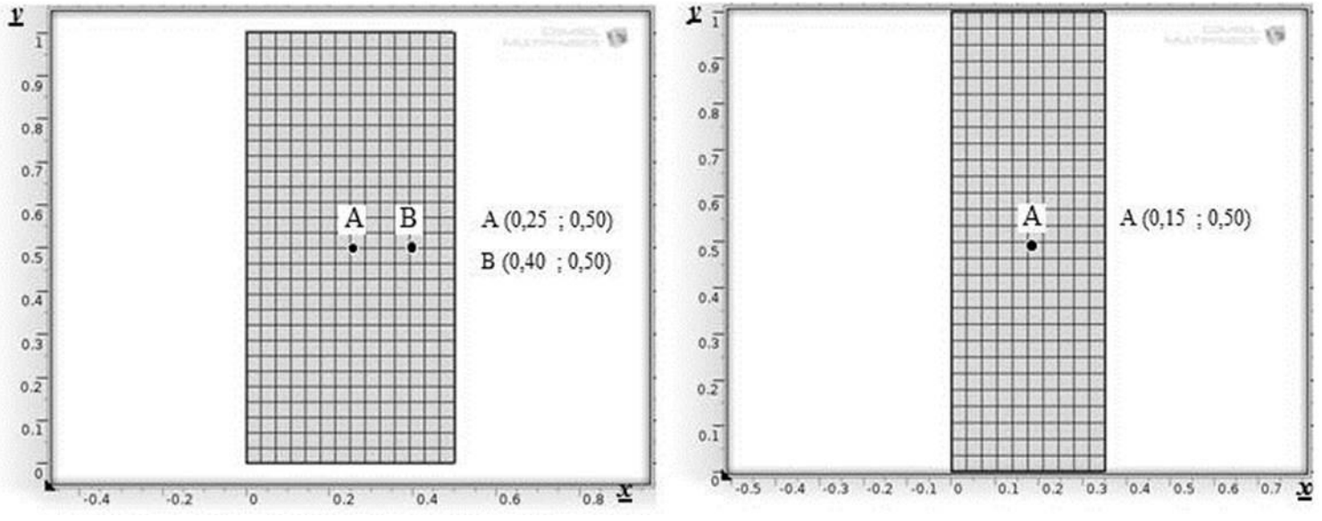

Figure 5

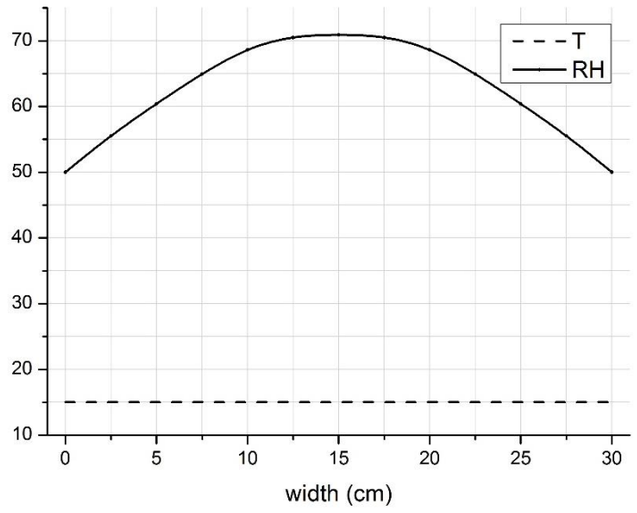

Figure 6

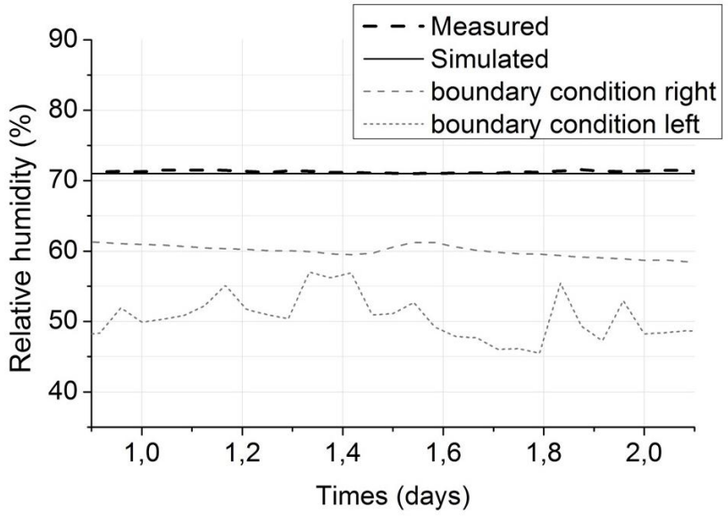

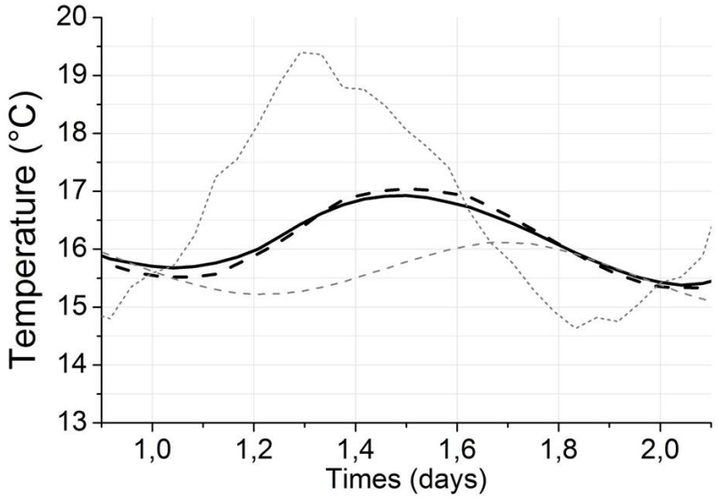

Figure 7

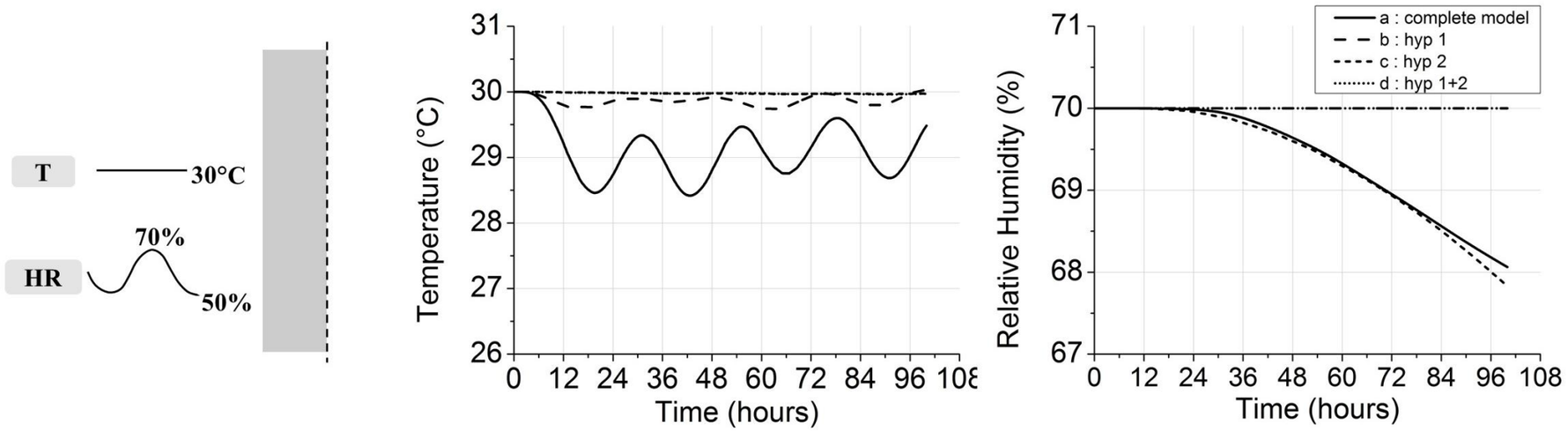

Figure 8

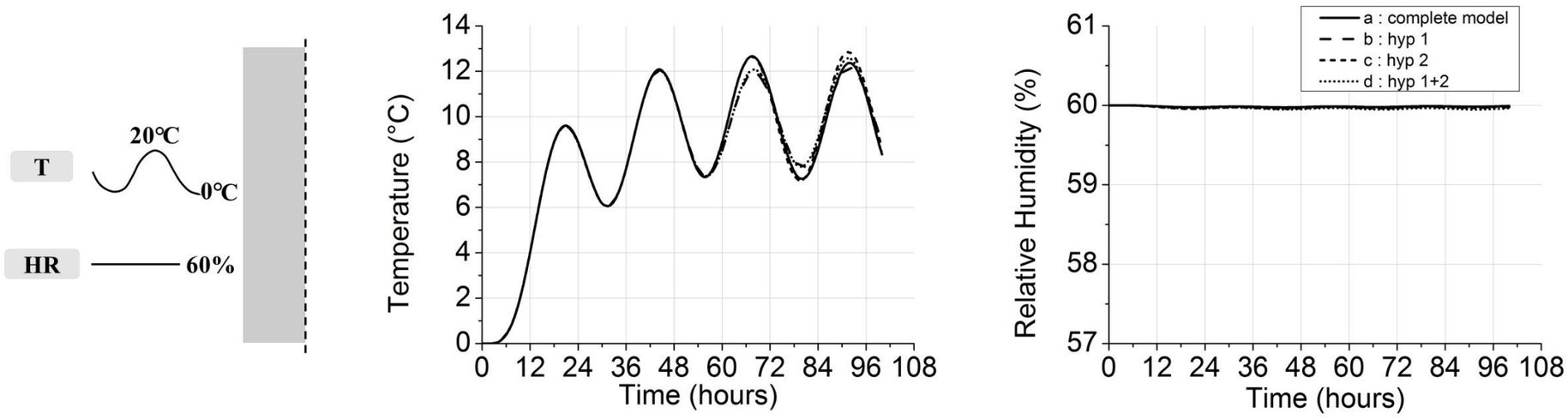

Figure 9

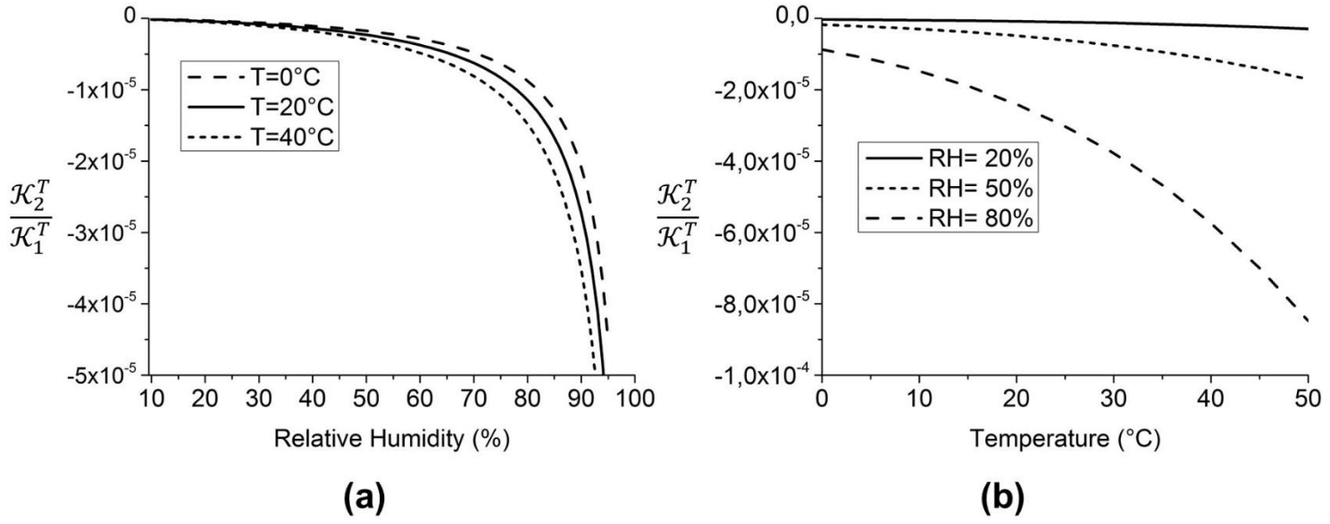

Figure 10

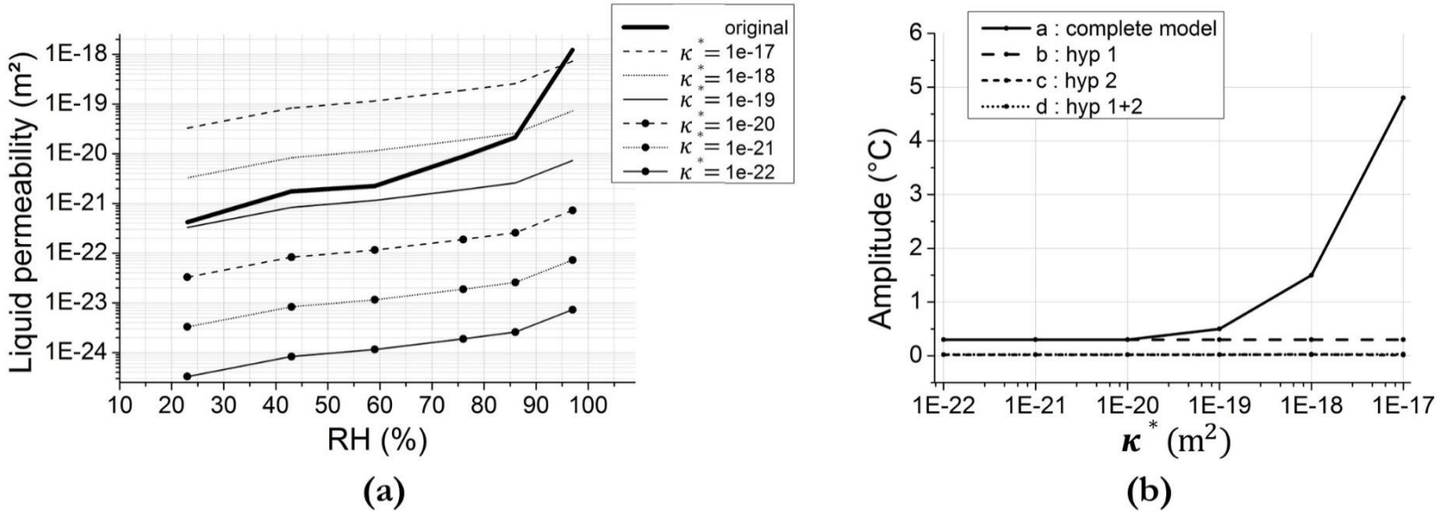

Figure 11

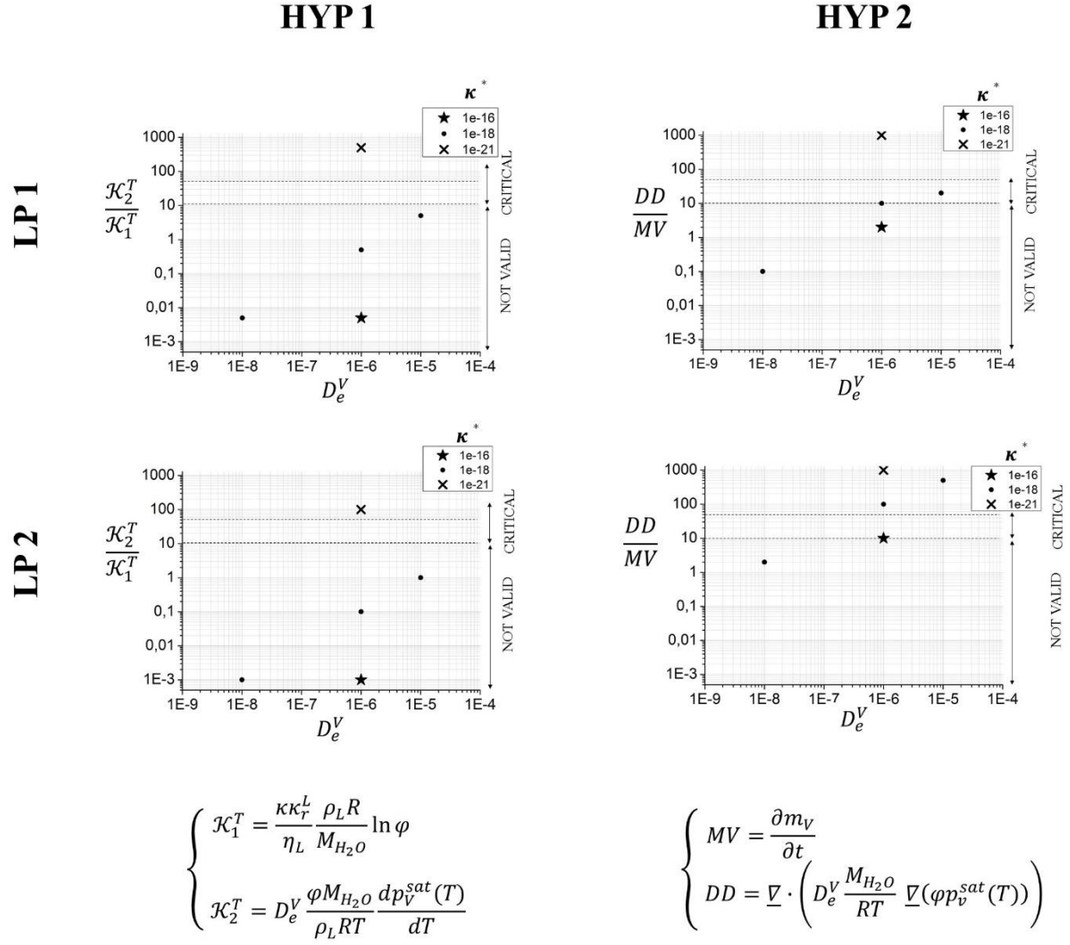

$$\begin{cases} \mathcal{K}_1^T = \dfrac{\kappa \kappa_r^L}{\eta_L} \dfrac{\rho_L R}{M_{H_2O}} \ln \varphi \\ \mathcal{K}_2^T = D_e^V \dfrac{\varphi M_{H_2O}}{\rho_L RT} \dfrac{dp_V^{sat}(T)}{dT} \end{cases}$$

$$\begin{cases} MV = \dfrac{\partial m_V}{\partial t} \\ DD = \underline{\nabla} \cdot \left(D_e^V \dfrac{M_{H_2O}}{RT} \underline{\nabla}(\varphi p_v^{sat}(T)) \right) \end{cases}$$

Figure1
Click here to download high resolution image

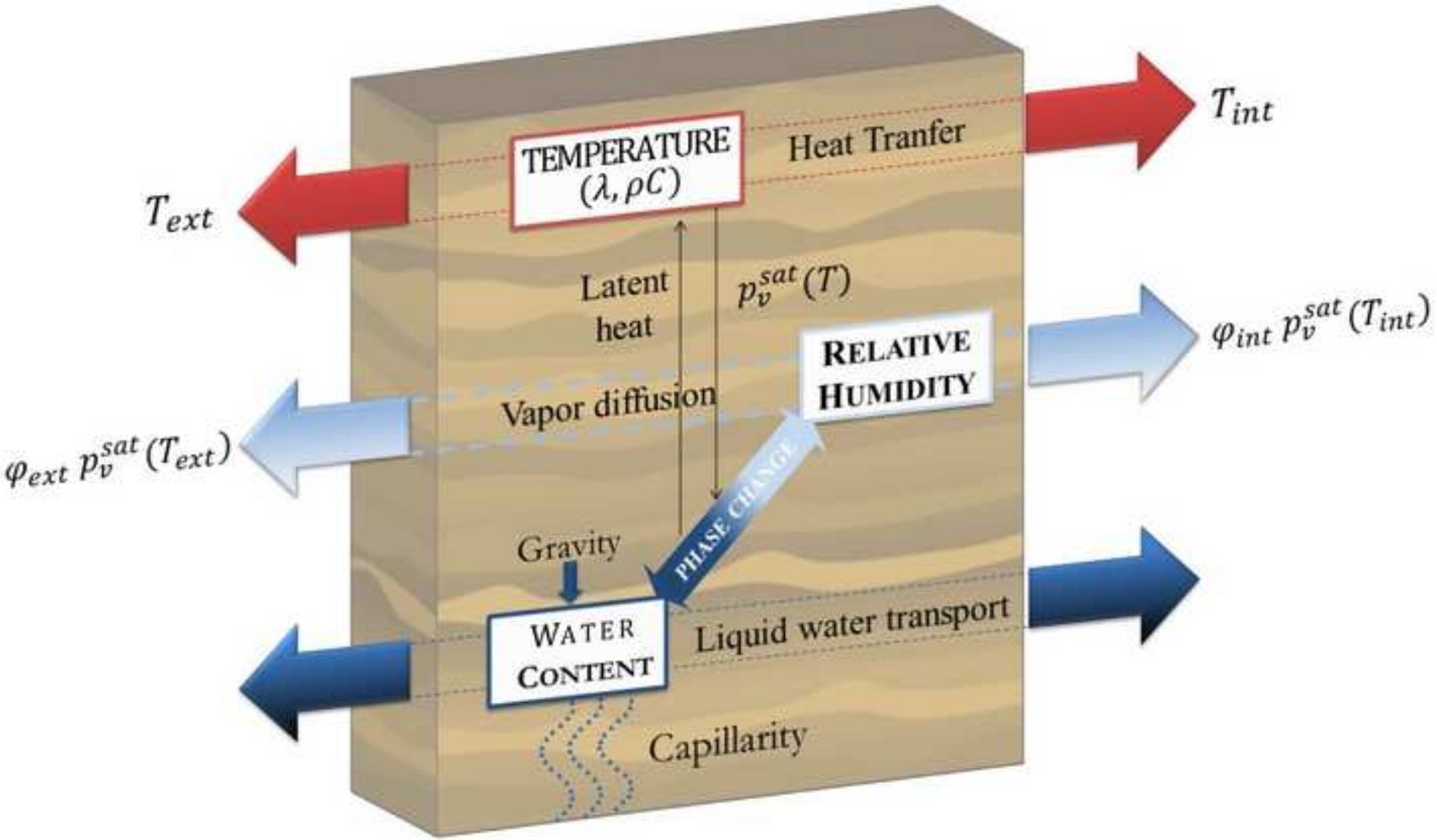

Figure2
Click here to download high resolution image

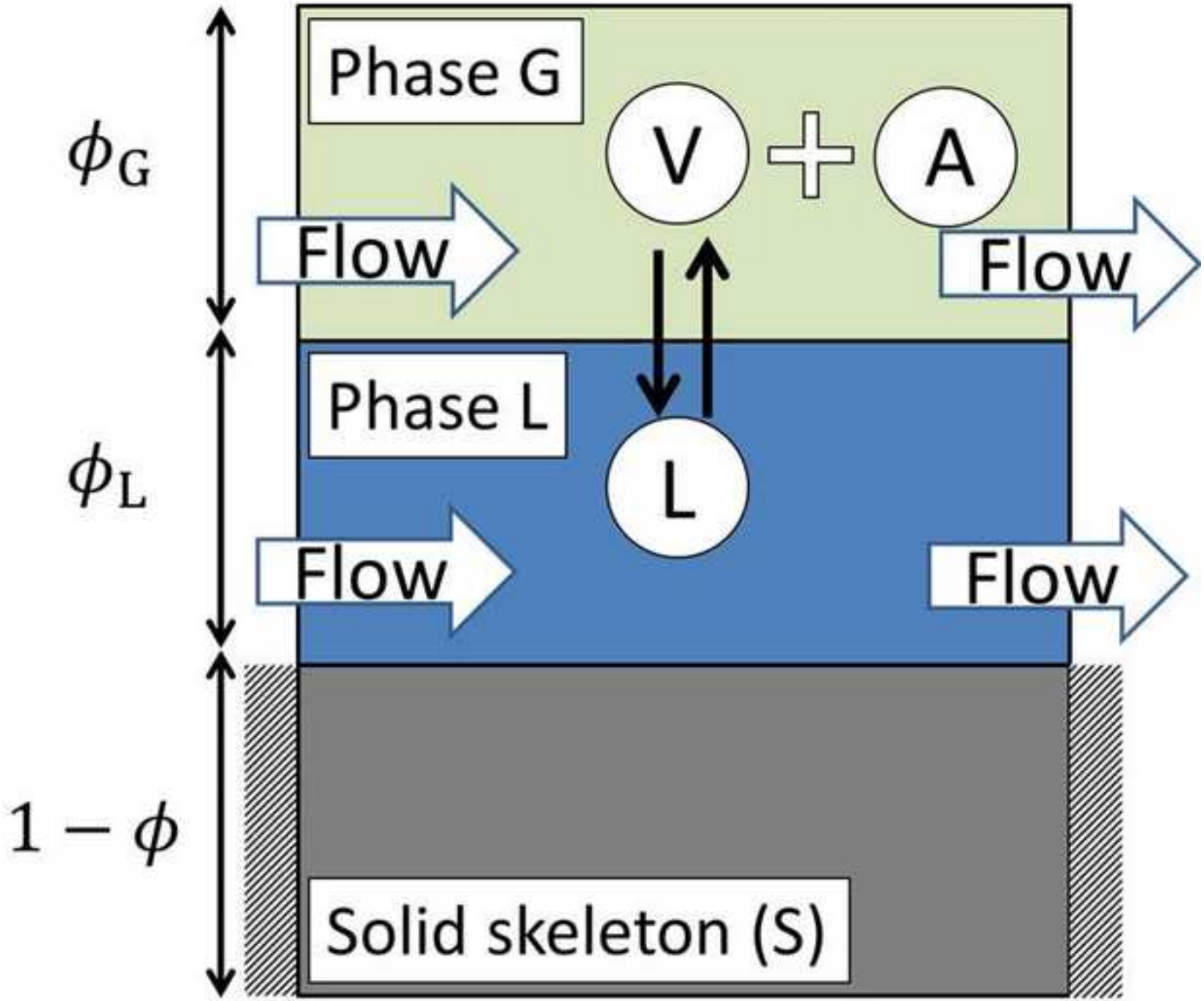

Figure3
Click here to download high resolution image

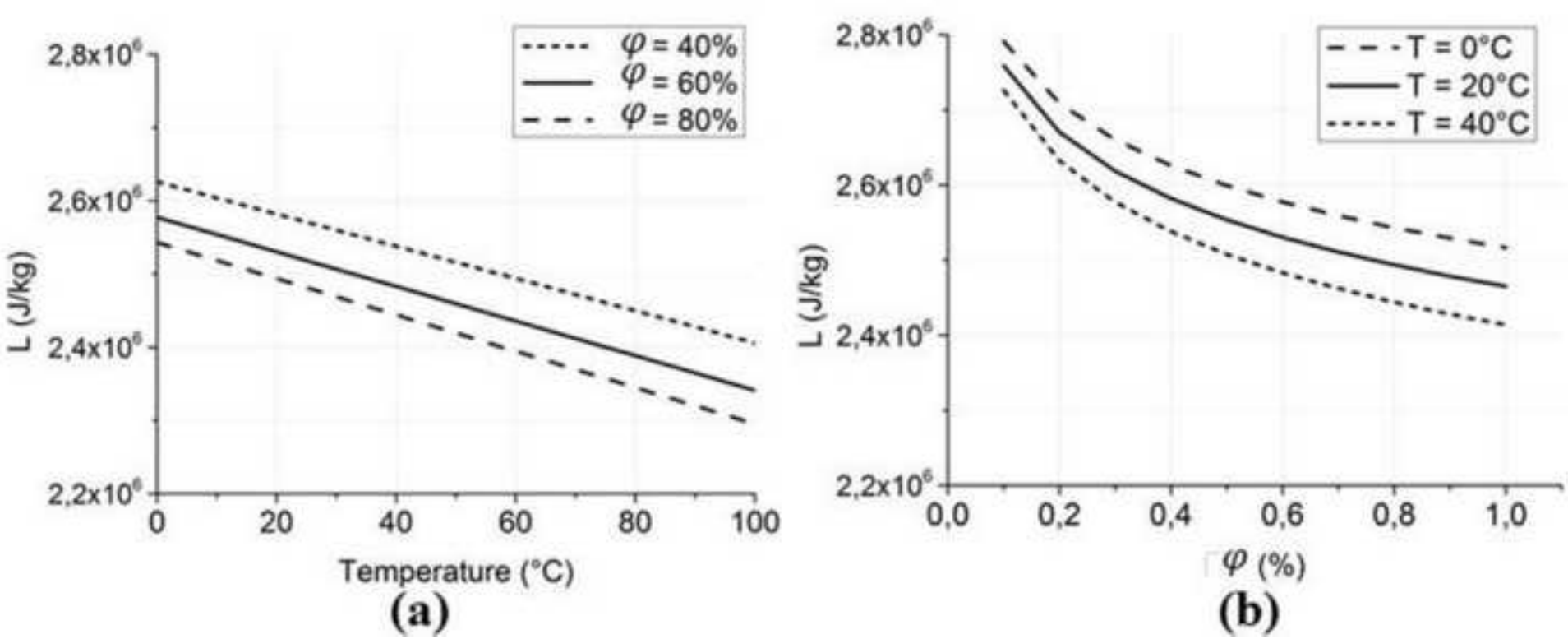

Figure4

Click here to download high resolution image

(a)

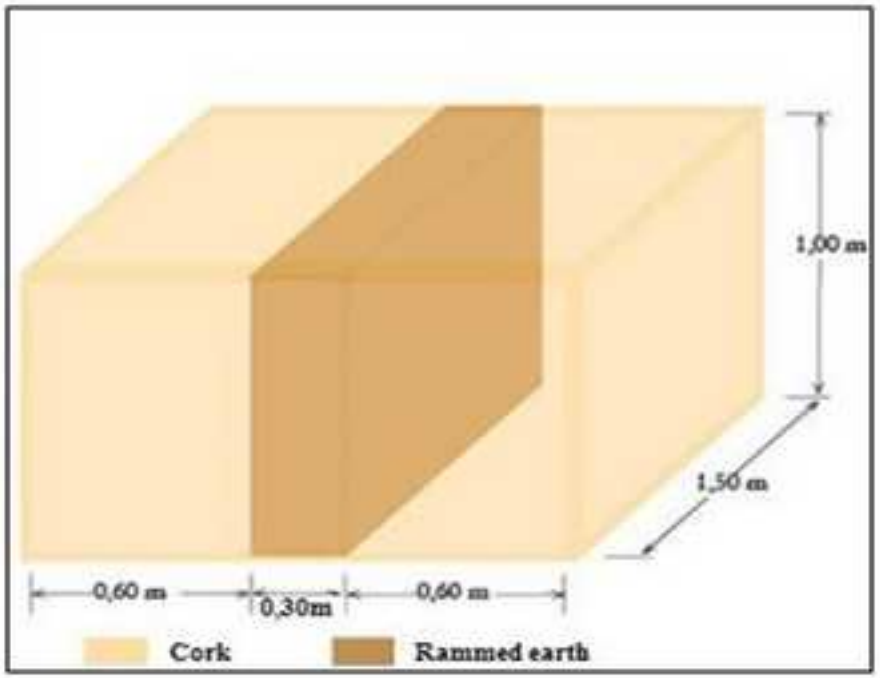

(b)

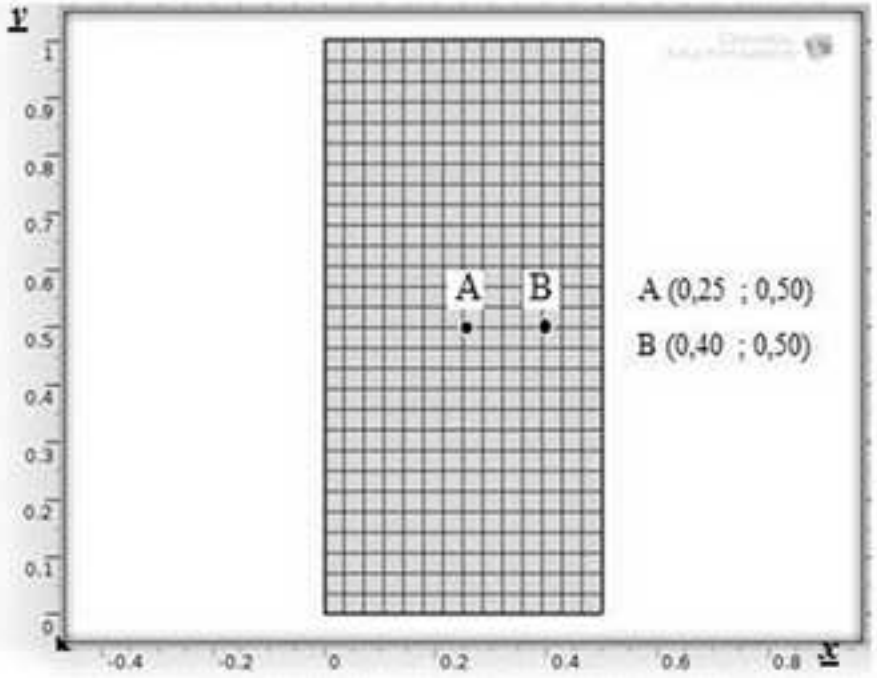

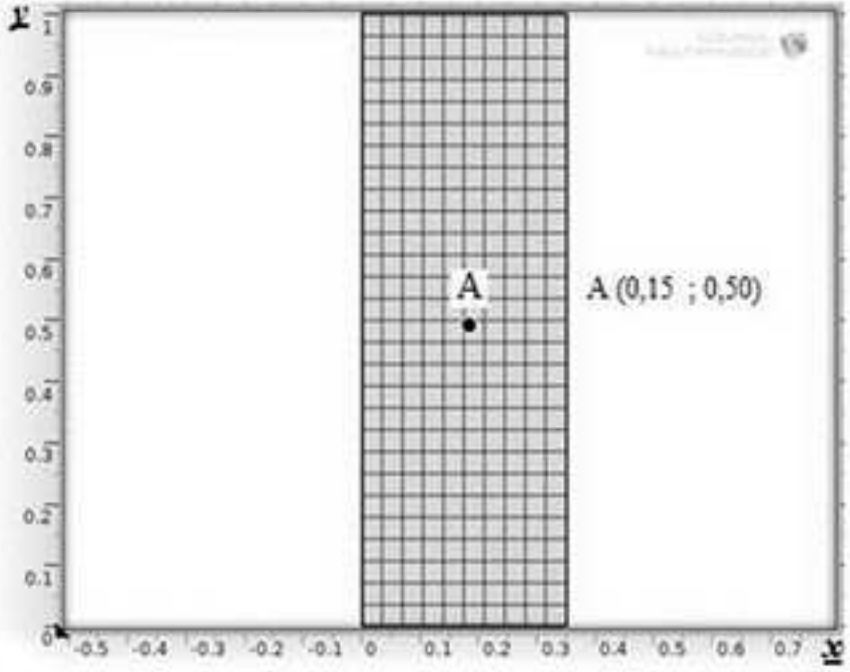

Figure5
Click here to download high resolution image

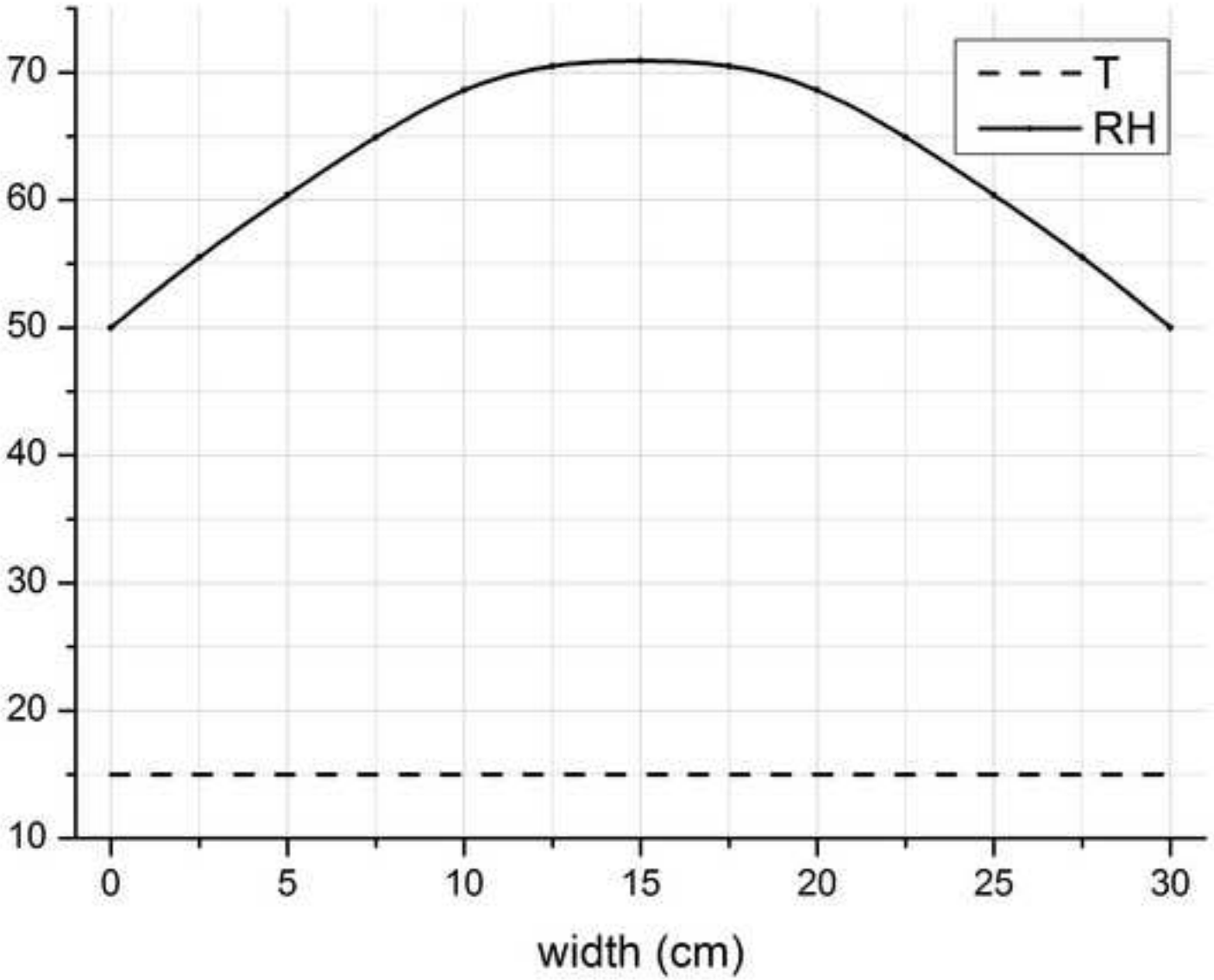

Figure6

Click here to download high resolution image

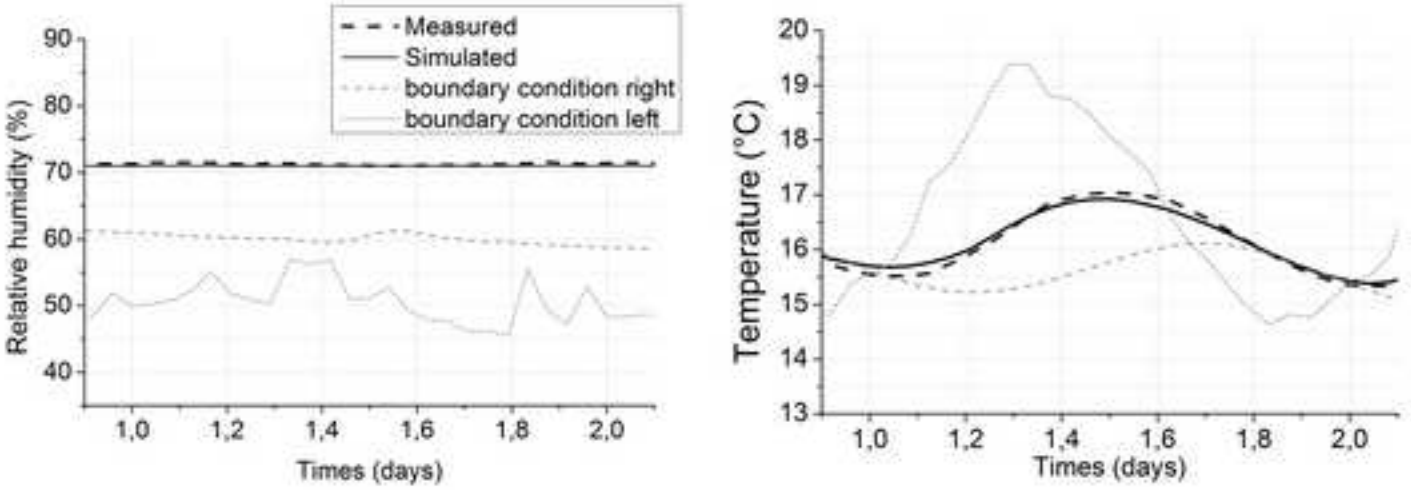

Figure7

Click here to download high resolution image

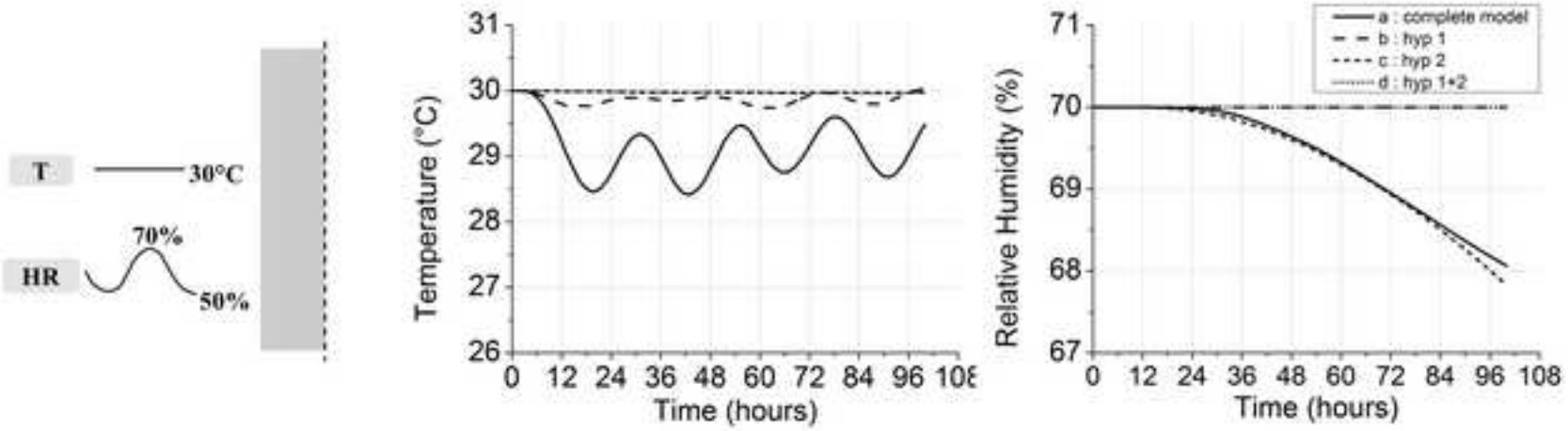

Figure8

Click here to download high resolution image

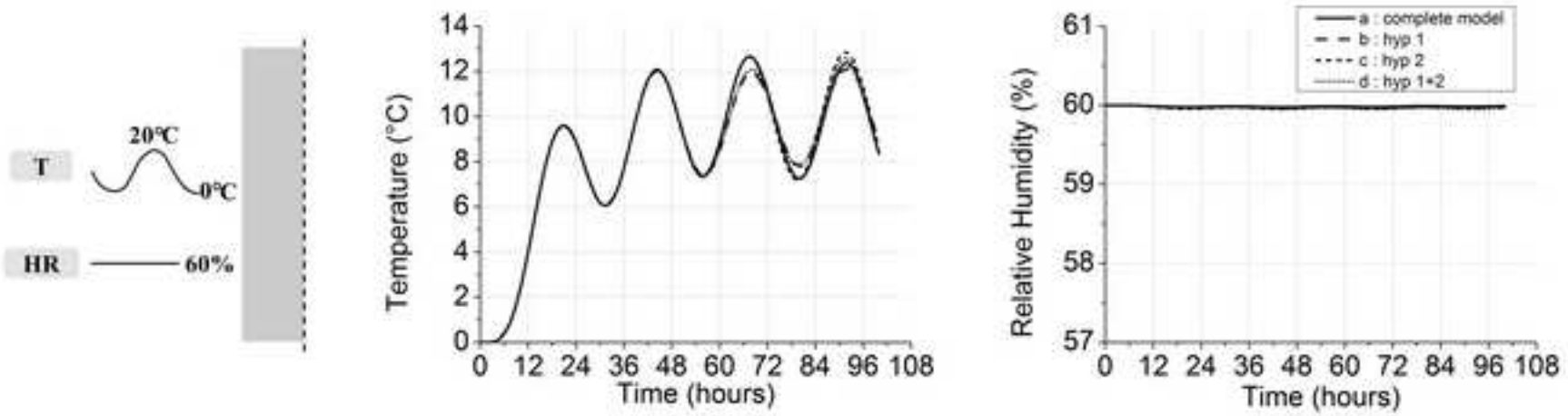

Figure9

Click here to download high resolution image

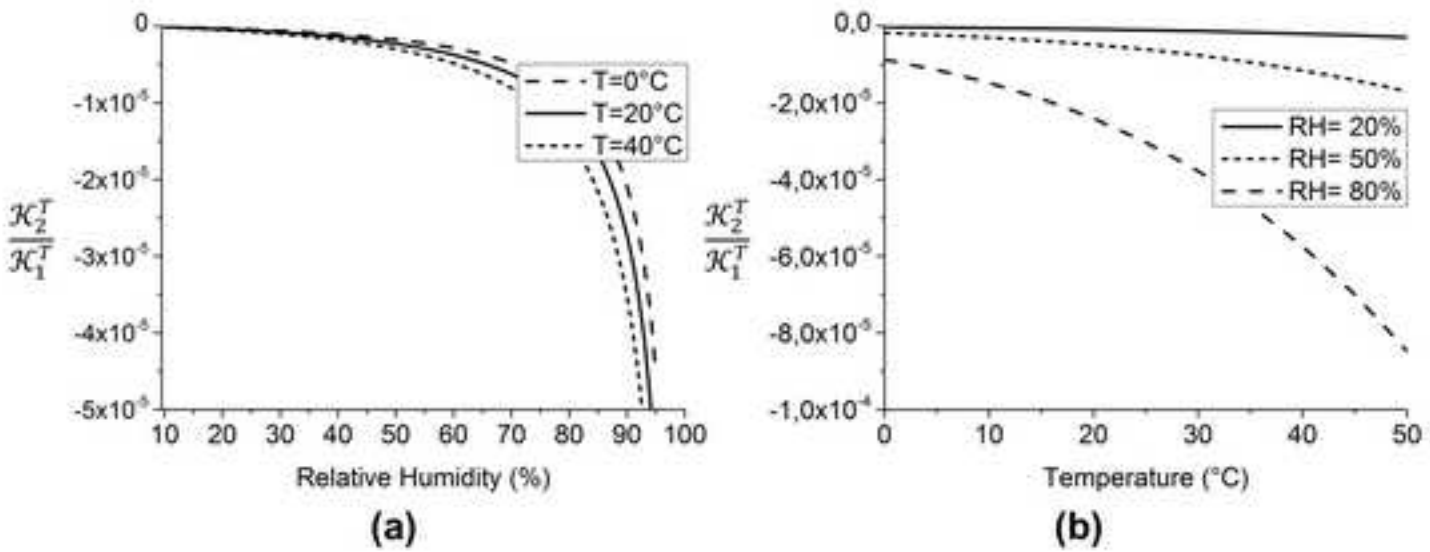

Figure10

Click here to download high resolution image

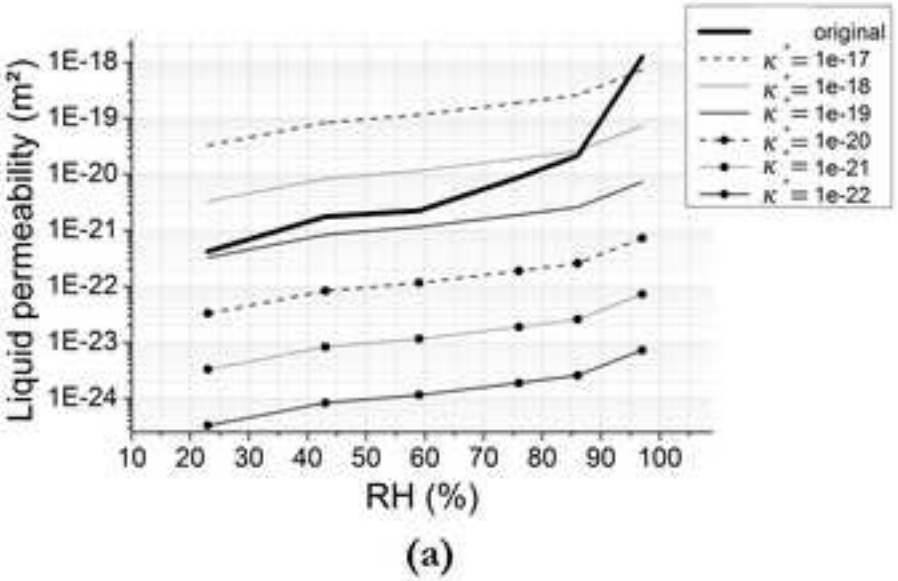

(a)

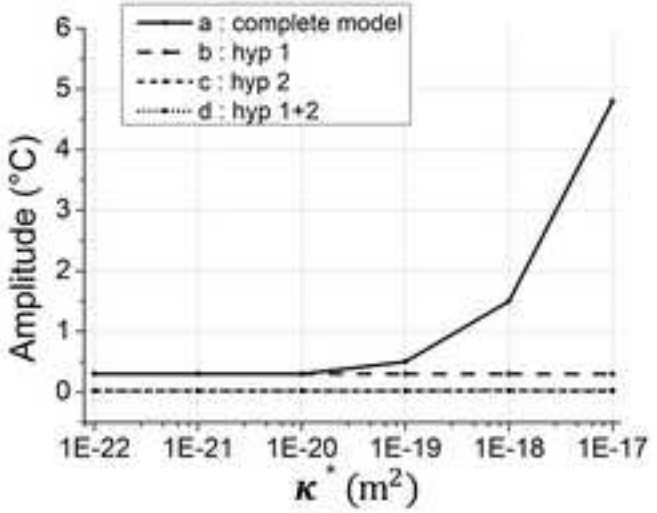

(b)

Figure11
Click here to download high resolution image

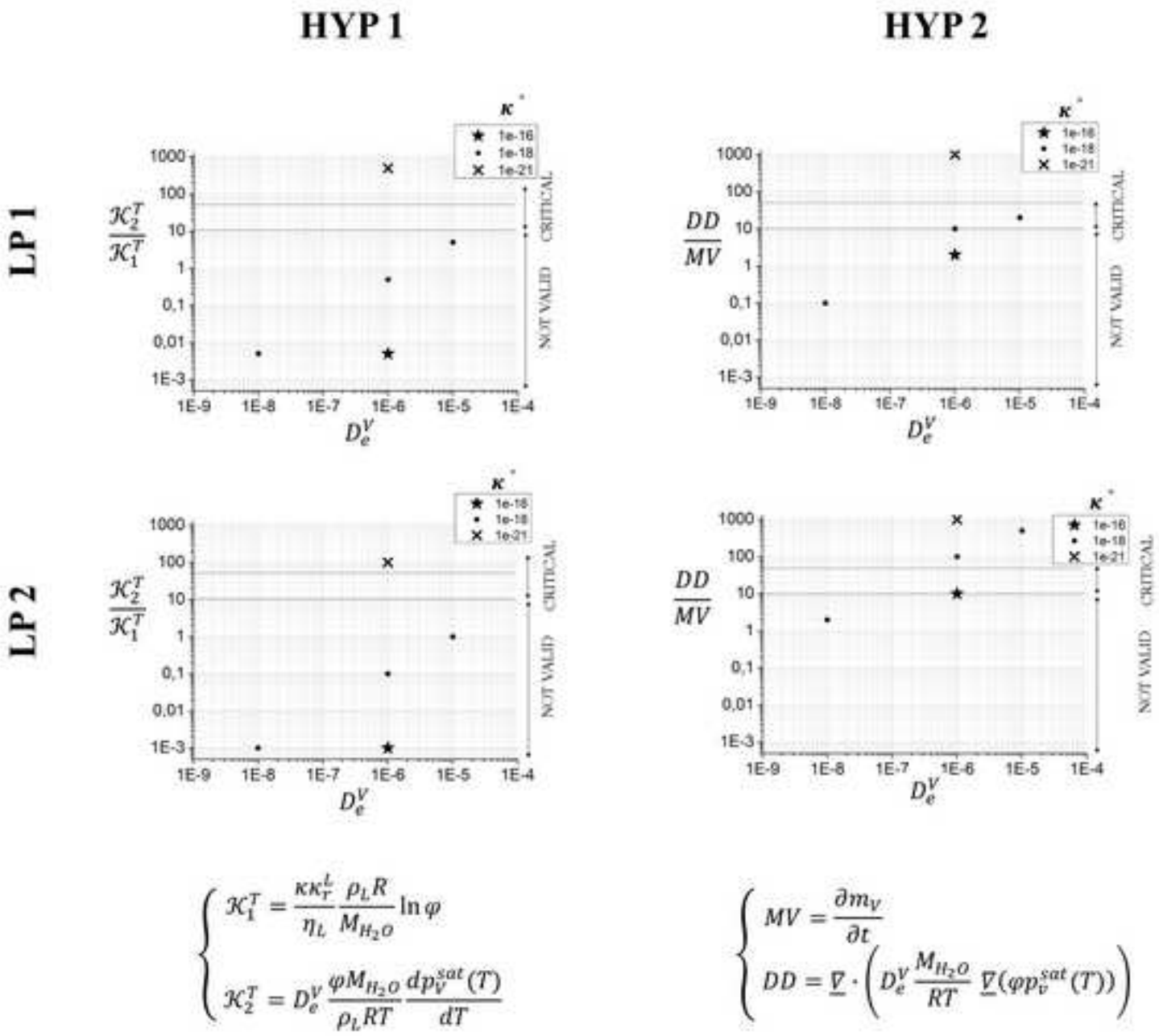

Table 4 Heat and water vapor flux for the complete model (a) and hyp 1+2 model (d) for loading paths LP1 and LP2.

	LP1		LP2	
	g_T^{max} [W.m^{-2}]	g_{RH}^{max} [kg.m^{-2}.s^{-1}]	g_T^{max} [W.m^{-2}]	g_{RH}^{max} [kg.m^{-2}.s^{-1}]
complete model (a)	12.4	-1.35.10^{-5}	62.7	-3.5.10^{-8}
Hyp 1 (b)	3.4	-1.70.10^{-5}	62.7	-6.6.10^{-8}
Hyp 2 (c)	0.02	-1.59.10^{-5}	64.3	-3.4.10^{-8}
hyp 1+2 (d)	0.14	-1.85.10^{-5}	64.3	-3.4.10^{-8}

Highlights

- A coupled hygrothermal model has been developed and implemented in COMSOL.
- The model is validated on experimental data of metric rammed earth wall.
- It is used to assess the accuracy of common simplifying assumptions.
- Some of these simplifications should not be done to model earthen materials.